burden. Ideally, changes in viable cell number result in proportional changes in light emission. In vitro experiments have demonstrated a linear relationship between cell numbers and light emission after the addition of D-luciferin to a dilution series of luciferase-expressing cells [3–7]. It has also been reported that the signal intensities obtained by in vivo bioluminescence imaging correlate positively with tumour burden in various animal models [3, 6, 8–19]. These observations support the use of bioluminescence imaging for quantitative evaluations of implanted tumour progression and regression. On the other hand, the activity of the CMV promoter has been shown to depend on the cell cycle stage and medium composition [20], and expression driven by the LTR has been suggested to decline under a stress condition [21]. It may be possible that alterations in the physiological status of the cell cause fluctuations in luciferase expression under the control of a constitutive promoter, thereby distorting the proportionality between viable cell number and bioluminescent signal intensity. It has not been fully examined whether luciferase activity increases with increasing viable cell number during disease progression or whether therapeutic interventions affect the level of luciferase activity per viable cell.

The Philadelphia chromosome (Ph) contains one of several types of BCR-ABL fusion gene and is important in the pathogenesis of both acute lymphoblastic leukaemia (ALL) and chronic myeloid leukaemia [22]. The BCR-ABL fusion proteins retain constitutive tyrosine kinase activity, leading to uncontrolled cell proliferation. Patients with Ph^+ ALL frequently express the p190 BCR-ABL fusion protein and have a very poor prognosis [23–25]. Although the BCR-ABL tyrosine kinase inhibitor, imatinib mesylate (STI571; Novartis Pharmaceuticals, Basel, Switzerland), is effective in the treatment of Ph^+ ALL patients [26], resistance to this drug develops rapidly, and novel therapeutic strategies to overcome the resistance need to be explored [27]. Since tumour cells may be distributed extensively and variably in leukaemia model animals, making it difficult to assess disease severity, whole-body, quantitative evaluation of tumour burden by in vivo bioluminescence imaging appears to have particular value [28].

The interleukin-3 (IL-3)-dependent murine pro-B cell line Ba/F3 [29] shows autonomous proliferation following transduction with the p190 BCR-ABL fusion gene [30]. In this study, we generated p190 BCR-ABL-transformed Ba/F3 cells stably expressing luciferase under the control of a retroviral LTR. Cell culture studies were conducted to investigate whether bioluminescent signal intensities could be used as indicators of cell proliferation and responses to imatinib. We cultured factor-dependent cells in the presence of different concentrations of IL-3 and measured the luciferase activities and viable cell numbers to evaluate the effect of IL-3 on luciferase expression. The proliferation of factor-independent cells was monitored serially by the luciferase assay and viable cell counting, and the relationship between them was defined, relative to the stage of proliferation. The effects of imatinib on luciferase activity and viable cell number were assessed to evaluate the reliability of bioluminescent monitoring of therapeutic responses. Our results indicate that changes in bioluminescent signal intensity generally reflect cell proliferation and therapeutic responses but differ, to some extent, from changes in viable cell number depending on cell conditions associated with proliferative activity.

Materials and methods

Cell lines

Ba/F3 cells were maintained in RPMI 1640 medium (Invitrogen, Grand Island, NY, USA) supplemented with 10% (v/v) fetal bovine serum (FBS; JRH Biosciences, Lenexa, KS, USA), 1% penicillin/streptomycin (Invitrogen) and 100–200 pg/ml recombinant murine IL-3 (mIL-3; kindly provided by Kirin Brewery, Maebashi, Japan). Ba/F3 cells transduced with the BCR-ABL genes were cultured in the absence of mIL-3. The culture density was kept below 5×10^5 cells/ml. A retrovirus-packaging cell line for ecotropic retroviruses, Plat-E [31], was maintained in Dulbecco's modified Eagle's medium (Invitrogen) supplemented with 10% FBS and 1% penicillin/streptomycin. The medium also contained 1 μg/ml puromycin (Sigma Chemical Co., St Louis, MO, USA) and 10 μg/ml blasticidin S (Funakoshi Co., Tokyo, Japan) as selection reagents. All of the cultures were incubated at 37°C and 5% CO_2.

Construction of plasmids and retroviral transduction

The cDNA encoding the firefly luciferase was excised from the pGL3-basic vector (Promega, Madison, WI, USA) and inserted into the retroviral vector pMX-neo [32], to generate pMX-luc/neo. The pMX-neo employs the LTR of Moloney murine leukaemia virus (MMLV) for the expression of inserted sequence and harbours a SV40 early promoter-driven neomycin resistance gene. The wild-type and mutant p190 BCR-ABL fusion genes were inserted into the retroviral vector pMC-Ig [32], to generate pMC-p190wt/Ig and pMC-p190mut/Ig, respectively. The pMC-Ig contains the enhanced green fluorescence protein (EGFP) gene downstream of the internal ribosome entry site. The mutant gene, which harbours the Y253H point mutation in the BCR-ABL kinase domain, was constructed by replacing the kinase domain of the wild-type cDNA with the corresponding mutated sequence derived from leukaemia cells from an imatinib-resistant Ph^+ ALL patient [33].

The luciferase expression plasmid pMX-luc/neo was transfected into Plat-E cells to generate the ecotropic retroviral vector. Plat-E cells (1.5×10^6 cells/3 ml) were seeded in a 60-mm dish, and pMX-luc/neo was transfected 16 h later using FuGENE 6 Transfection Reagent (Roche Diagnostics, Indianapolis, IN, USA) according to the manufacturer's protocol. The culture supernatants were harvested 48 and 72 h after transfection, and Ba/F3 cells were transduced in the presence of polybrene. The infected Ba/F3 cells were selected for 14 days with 1.0 mg/ml G418 (Calbiochem, San Diego, CA, USA) and termed Ba/F3-Luc cells. Similarly, the Ba/F3-Luc cells and parenteral Ba/F3 cells were transduced with pMC-p190wt/Ig or pMC-p190mut/Ig. The infected cells were selected by IL-3 depletion for 14 days. The Ba/F3-Luc cells transduced with the wild-type and mutant p190 genes were referred to as Ba/F3-Luc/Wt and Ba/F3-Luc/Mut cells, respectively.

In vitro analysis

The standard luciferase assay, intact-cell luciferase assay, viable cell counting and cell cycle analysis were performed to assess the bioluminescent features and proliferative status of cultured cells. All measurements were done in triplicate. The viable cell numbers were measured using the trypan blue dye exclusion method and a haemocytometer. For comparisons of sensitivities to imatinib between cell lines, a cell titre assay was performed using the WST-8 assay kit (TetraColor One; Seikagaku Co., Tokyo, Japan) according to the manufacturer's recommendations.

Luciferase activity in a given volume of cell suspension was determined by the standard luciferase assay. To prepare the lysate, 100 µl of cell suspension was transferred from a cell culture plate to a microtube and centrifuged on a tabletop centrifuge (2,000 rpm, 5 min). The pellet was lysed with 200 µl of lysis buffer (Passive Lysis Buffer; Promega). The lysate was centrifuged, and the supernatant was stored at −80°C until assayed. Luminescence from the lysate was measured using the Luciferase Assay Reagent (Promega) according to the manufacturer's recommendation and using a plate reader (Wallac ARVO MX 1420 Multilabel Counter; Perkin Elmer Japan, Yokohama, Japan). In some experiments, luminescence was also measured by simply adding D-luciferin (Beetle Luciferin Potassium Salt; Promega) to the cell suspension without cell lysis. We referred to this latter assay as the intact-cell luciferase assay. Cell suspension (50 µl) was transferred to a white 96-well cell culture plate. One minute after the addition of D-luciferin (10 µl of 600 µg/ml solution) to the cell suspension, the light output was measured using the plate reader. Phenol red-free RPMI 1640 medium was used to avoid possible light absorbance by the dye. For both the standard and the intact-cell luciferase assay, luminescence per cell (counts per second/cell; cps/cell) was calculated from the mean luminescence and mean viable cell number. The measurements of luminescence using the plate reader were performed at 25°C.

To assess the cell cycle, cells were fixed with cooled 70% ethanol. Afterwards, the fixed cells were washed twice with phosphate-buffered saline and incubated with 0.5% ribonuclease A for 30 min. After the addition of propidium iodide (final concentration, 50 µg/ml), the cells were analysed by flow cytometry using the FACSCalibur flow cytometer (Beckton Dickinson, Franklin Lakes, NJ, USA). The cell cycle was analysed using the FlowJo software (TreeStar, San Carlos, CA, USA). The fraction of proliferating cells, or proliferation index, was calculated by the following equation: proliferation index (%)=$(G_2/M+S)/(G_1/G_0+G_2/M+S)\times100$, where G_2/M, S and G_1/G_0 are the numbers of cells in the G_2/M, S and G_1/G_0 phases, respectively.

In vivo bioluminescence imaging

Two female wild-type BALB/c mice were inoculated subcutaneously in the right femoral region with 1×10^5 Ba/F3-Luc/Wt cells. Five minutes later, the mice received an intraperitoneal injection of 150 mg/kg D-luciferin and placed in the light-tight chamber of a cooled CCD camera system (IVIS Imaging System 100; Xenogen, Alameda, CA, USA) in the prone position under isoflurane anaesthesia. Photographic and luminescent images were acquired 20 min after D-luciferin injection using the CCD camera system. In addition, two female BALB/c *nu/nu* mice were injected intravenously with 2×10^6 Ba/F3-Luc/Wt cells, followed 10 min later with injection of D-luciferin. Dorsal, left lateral, ventral and right lateral images were acquired from 10 min after D-luciferin injection with the CCD camera system. All luminescent images were collected with an exposure time of 1 min and binning of 8. Mice were handled according to the guidelines of the Institute of Medical Science, University of Tokyo. The experiments were approved by the committee for animal research at the institution.

Results

Generation of factor-independent Ba/F3 cell lines expressing luciferase

We transduced Ba/F3 cells with firefly luciferase genes using a retroviral vector, then selected with G418, and confirmed that the cells expressed luciferase. We then transduced the obtained luciferase-expressing Ba/F3-Luc cells and parental Ba/F3 cells with wild-type or mutant p190 BCR-ABL fusion genes, to give IL-3-independent, autonomous cellular proliferation. A clone from each of the four cell lines was selected for further investigation based on the presence of a single peak of EGFP expression on flow cytometry and, for luciferase-expressing cells, strong expression of luciferase.

The cell growth curves, determined by viable cell counting, were similar for the four cell lines (data not shown), and no significant effect of luciferase expression on the proliferation rate was noted. For the evaluation of sensitivity to imatinib, we cultured the four cell lines in the presence of various concentrations of imatinib (0–10 µ*M*) and performed the standard cell titre assay. The dose-response curves demonstrated the sensitivity of Ba/F3-Luc/Wt cells and resistance of Ba/F3-Luc/Mut cells to imatinib (data not shown). The transduction with luciferase genes did not influence sensitivity to imatinib. Furthermore, luciferase expression by Ba/F3-Luc/Wt cells maintained in the absence of G418 was assessed repeatedly. The standard luciferase assay and viable cell counting were performed 24 h after replating. The luminescence per cell remained constant (range 159.6–167.0 cps/cell) from 5 to 39 days after thawing the frozen cell stock, which indicates excellent long-term stability of luciferase expression even in the absence of selection pressure.

In vivo bioluminescence imaging

We examined the detectability of the luciferase-expressing cells by in vivo bioluminescence imaging. For the mice inoculated subcutaneously with 1×10^5 Ba/F3-Luc/Wt cells, light emission was clearly detected at the site of cell implantation (Fig. 1a). For the mice injected intravenously with 2×10^6 Ba/F3-Luc/Wt cells, light emission was detected throughout the body (Fig. 1b,c), indicating diffuse distribution of the injected cells. Relatively strong signals were shown for the lung, liver and spleen.

Luminescence in dilution series

To assess the relationship between bioluminescent signal intensity and viable cell numbers, we prepared a dilution

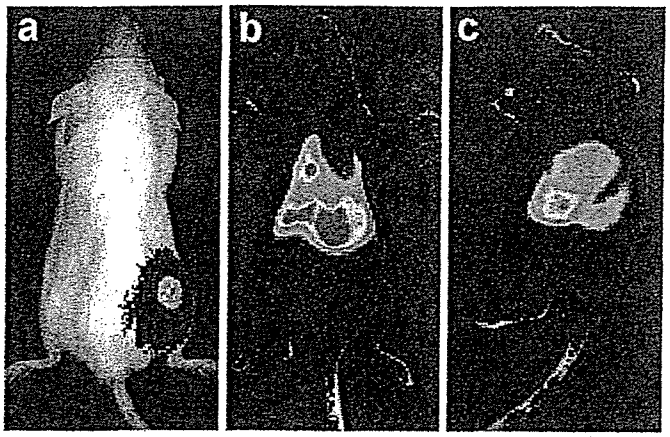

Fig. 1. In vivo bioluminescence images after inoculation of Ba/F3-Luc/Wt cells. The pseudocolour luminescent image (blue, green, yellow and red from the weakest to the strongest) is overlaid on the grey-scale photographic image. After subcutaneous inoculation in the right femoral region of the mouse, light emission is shown at the site of inoculation on the dorsal image (**a**). Following intravenous inoculation, the ventral (**b**) and left lateral (**c**) images reveal extensive light emission, particularly at the sites corresponding to the lung, liver and spleen

series of the Ba/F3-Luc/Wt cells (range 2.5×10^4–1.6×10^6 cells/ml) and measured the luminescence for a given volume of cell suspension using the standard and intact-cell luciferase assays. For the standard luciferase assay, the luminescence increased in proportion to the increasing cell numbers (Fig. 2a) and the luminescence per cell was constant, irrespective of cell number (range 195.3–201.5 cps/cell). Luminescence measured by the intact-cell luciferase assay was also highly proportional to cell number (Fig. 2b), and the luminescence per cell was stable (range 1.467–1.571 cps/cell). All of the following assays were performed in the linear range.

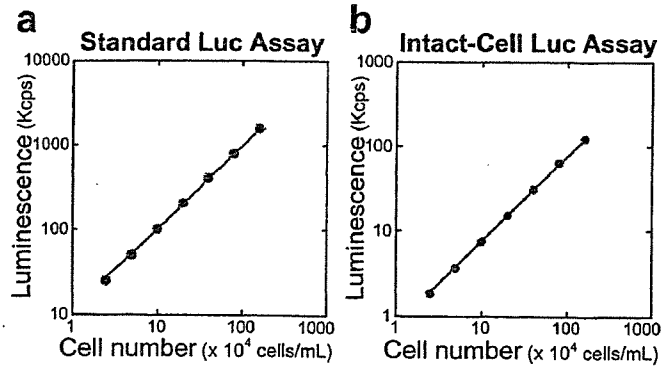

Fig. 2. Relationship between cell number and luminescence in a cell dilution series. The levels of luminescence in the standard luciferase assay (**a**) and in the intact-cell luciferase assay (**b**) were highly proportional to the numbers of Ba/F3-Luc/Wt cells prepared by serial dilution. Error bars are not visible because the standard errors are too small

IL-3 levels and luciferase activities

We evaluated the effects of mIL-3 on cell proliferation and luciferase expression for factor-dependent Ba/F3-Luc cells, not expressing BCR-ABL. After 24-h incubation in the presence of different concentrations of mIL-3 (100, 10 and 1 pg/ml), viable cell numbers, luciferase activities in the standard luciferase assay and proliferation indices were determined. The viable cell number increased with increasing mIL-3 concentration, indicating dose-dependent stimulation of cell proliferation (Fig. 3a). Luminescence for a given volume of cell suspension also increased with increasing mIL-3 concentration (Fig. 3b). The dependence on mIL-3 concentration was more prominent for luminescence than for viable cell number, and thus luminescence per cell increased with increasing mIL-3 concentration (Fig. 3c), which suggests enhancement of luciferase expression by mIL-3. The proliferation index was higher for 100 pg/ml mIL-3, consistent with higher proliferative activity, than for 10 pg/ml or 1 pg/ml (Fig. 3d).

Monitoring of proliferation by luciferase assays

To investigate the validity of bioluminescent signal as a marker of cell proliferation, we evaluated the proliferation of factor-independent cells, Ba/F3-Luc/Wt cells and Ba/F3-Luc/Mut cells, by serial assessments of viable cell numbers, luminescence in the standard luciferase assay, luminescence in the intact-cell luciferase assay and proliferation indices. The culture medium was not changed after replating, and measurements were performed every 12 h. No substantial differences were found between the Ba/F3-Luc/Wt and Ba/F3-Luc/Mut cells (data not shown). The viable cell numbers increased rapidly and then reached a plateau (Fig. 4a). As for the standard luciferase assay, luminescence for a given volume of cell suspension increased during the proliferative phase, which suggests that this assay provides an indicator of cell proliferation. However, increases in luminescence tended to be less prominent than increases in viable cell number, implying a mild underestimation of proliferation by the standard luciferase assay. During the plateau phase, luminescence decreased despite constant viable cell numbers, and a discrepancy was noted between the proliferation assessed by viable cell counting and that assessed using the standard luciferase assay. Luminescence per cell for the standard luciferase assay showed a gradual reduction over time, suggesting an incubation time-dependent decline in luciferase expression (Fig. 4b). The cell cycle analysis also demonstrated a gradual decline in proliferation index, and the time course was similar between the luciferase activity per cell and the proliferative fraction (Fig. 4c). The increase in luminescence seen in the intact-cell luciferase assay was more pronounced than that in the standard luciferase assay and closely paralleled the increase in viable cell numbers during the proliferative phase (Fig. 4a). During the plateau phase, a discrepancy between viable cell counting and the intact-cell luciferase assay occurred to a lesser degree than

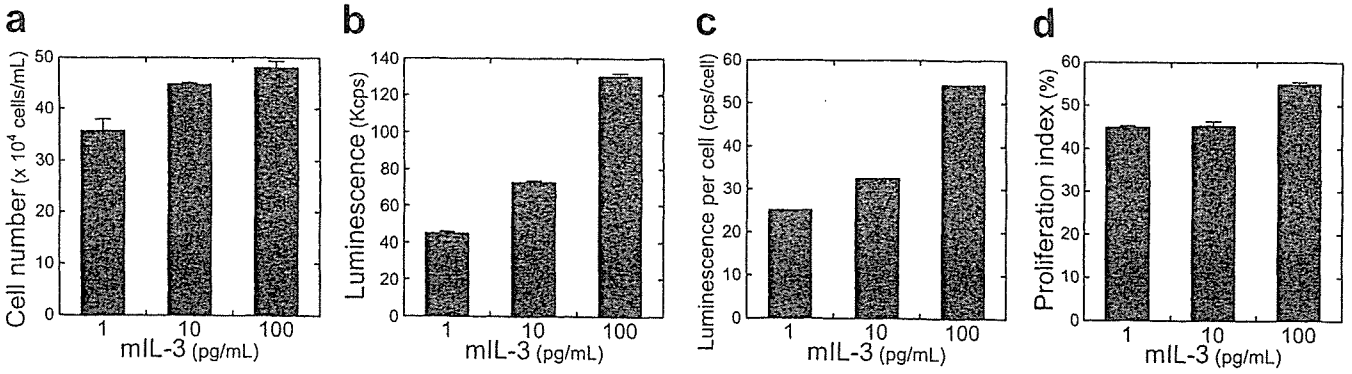

Fig. 3. IL-3 concentration and luciferase activity. Factor-dependent Ba/F3-Luc cells (1×10^5 cells/ml) were seeded in a 24-well plate in the presence of different concentrations of mIL-3. After 24 h, the viable cell number (**a**), luminescence in the standard luciferase assay (**b**), luminescence per cell (**c**) and proliferation index (**d**) were determined for each well. IL-3 dependence was more pronounced for luminescence than for viable cell number, and luminescence per cell increased with increasing concentrations of mIL-3. *Error bars* in panels **a**, **b** and **d** represent standard errors

between viable cell counting and the standard luciferase assay. The incubation time-dependent decrease in luminescence per cell for the intact-cell luciferase assay was evident but less prominent than that for the standard luciferase assay (Fig. 4b).

Monitoring of responses to imatinib by luciferase assay

We assessed the effect of imatinib on cell proliferation and luciferase activity for factor-independent cells. After 24-h incubation of Ba/F3-Luc/Wt cells in the presence of 1.0, 0.5, 0.25 or 0 μ*M* imatinib, viable cell counting, standard luciferase assay, and cell cycle analysis were performed. The presence of 1 μ*M* imatinib mildly depressed the increase in viable cell numbers (Fig. 5a), while such an inhibitory effect was not evident with 0.5 μ*M* or 0.25 μ*M* imatinib. Luciferase activity assessed by the standard luciferase assay was reduced even at 0.25 μ*M* when compared with the corresponding value in the absence of imatinib, and further decreased in a dose-dependent manner (Fig. 5b). The decrease in luciferase activity was more pronounced than that for viable cell number, and thus luminescence per cell was also reduced by the increasing imatinib concentration (Fig. 5c). The cell cycle analysis revealed dose-dependent decreases in the proliferative fraction (Fig. 5d). For the Ba/F3-Luc/Mut cells, which are resistant to imatinib, the presence of 1 μ*M* imatinib had no substantial effect on viable cell number, luciferase activity, luminescence per cell or proliferative fraction (data not shown).

We sequentially assessed the proliferation of Ba/F3-Luc/Wt cells in the presence or absence of 1 μ*M* imatinib. The measurements, including viable cell counting, standard luciferase assay and cell cycle analysis, were performed immediately after the addition of imatinib and every 12 h thereafter. Although time-dependent increases in viable cell number (Fig. 6a) and luminescence in the standard luciferase assay (Fig. 6b) were demonstrated in the presence and absence of imatinib, the increases were attenuated in the presence of imatinib. The inhibitory effect on viable cell number was not apparent 12 h after the

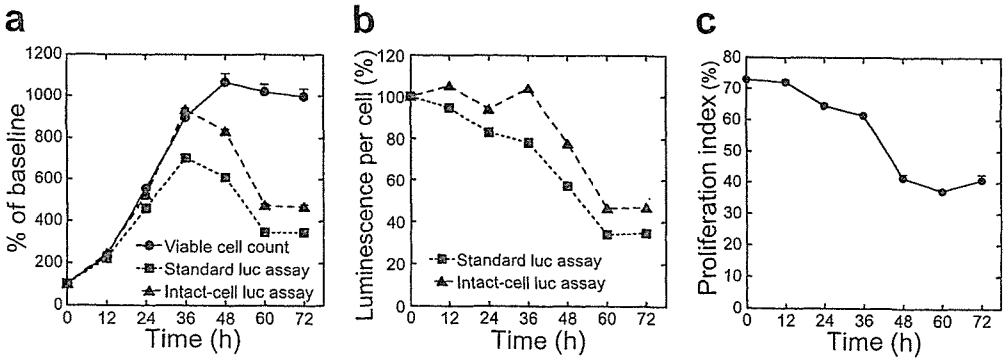

Fig. 4. Monitoring of proliferation of Ba/F3-Luc/Wt cells by luciferase assays. The cells (5×10^4 cells/ml) were seeded in a 24-well plate, and measurements were performed every 12 h after a 12-h pre-incubation period. The viable cell numbers and luminescence values from the standard luciferase assay and from the intact-cell luciferase assay, expressed as percentages of baseline values, increased over incubation time (**a**), and the luciferase assays reflected cell proliferation during the proliferative phase. However, definite underestimation occurred during the plateau phase and was more pronounced for the standard luciferase assay than for the intact-cell luciferase assay. Luminescence per cell (**b**) and proliferation index (**c**) decreased over time. *Error bars* in panels **a** and **c** represent standard errors

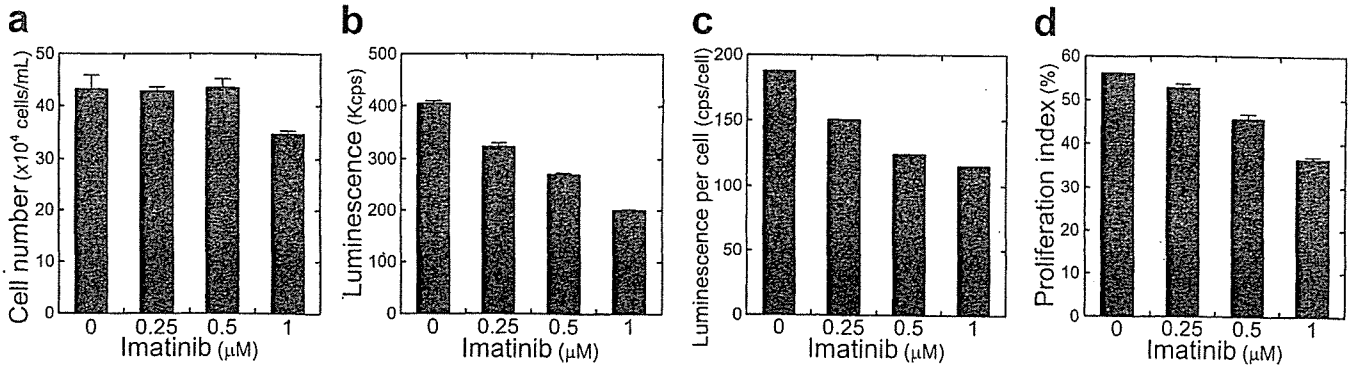

Fig. 5. Imatinib concentration and luciferase activity. The Ba/F3-Luc/Wt cells (1×10^5 cells/ml) were seeded in a 24-well plate with different concentrations of imatinib. After 24 h, the viable cell number (**a**), luminescence in the standard luciferase assay (**b**), luminescence per cell (**c**) and proliferation index (**d**) were determined. Increases in imatinib concentration decreased all measures. The effect was more pronounced on luminescence than on viable cell number. *Error bars* in panels **a**, **b** and **d** represent standard errors

addition of imatinib, but became evident at 24 h. The inhibitory effect on luciferase activity was evident even at 12 h and was more pronounced than that on cell number. Luminescence per cell showed a definite decline over time in the presence of imatinib, while it was almost constant in the absence of imatinib during the observation period (Fig. 6c). The proliferation index at 12 h was almost equal to that at baseline, irrespective of the presence or absence of imatinib (Fig. 6d). Otherwise, the time course for the proliferation index resembled that for luminescence per cell.

Discussion

In vivo bioluminescence imaging offers a promising tool for small animal experiments. In this study, we generated p190-BCR-ABL-transduced Ba/F3 cells, which were either sensitive or resistant to imatinib, for monitoring by in vivo bioluminescence imaging. Since bioluminescent monitoring of tumour models requires stable expression of luciferase, we introduced the firefly luciferase gene under the control of the MMLV LTR, a representative constitutive promoter. No substantial differences in proliferation rate or responsiveness to imatinib were found between the cell lines with and without the luciferase gene, justifying the prediction of proliferation and treatment responses of cells that do not express luciferase, based on those of cells that stably express luciferase. Although it is possible to maintain stable gene expression in cell cultures using selection agents, stable expression of luciferase in the absence of selection pressure is needed for in vivo use. We confirmed the long-term stability of luciferase expression in medium not containing selection agents. We imaged mice using a CCD camera after subcutaneous or intravenous inoculation of the luciferase-expressing Ba/F3 cells and demonstrated the feasibility of visualising the cells, located either superficially or deeply, by in vivo bioluminescence imaging. In vivo light signal was clearly detected for wild-type mice coated with white fur as well as for nude mice. Luciferase expression in the cells is considered to be sufficient for in vivo imaging. These in vitro and in vivo results suggest that the cells established here have characteristics suitable for the

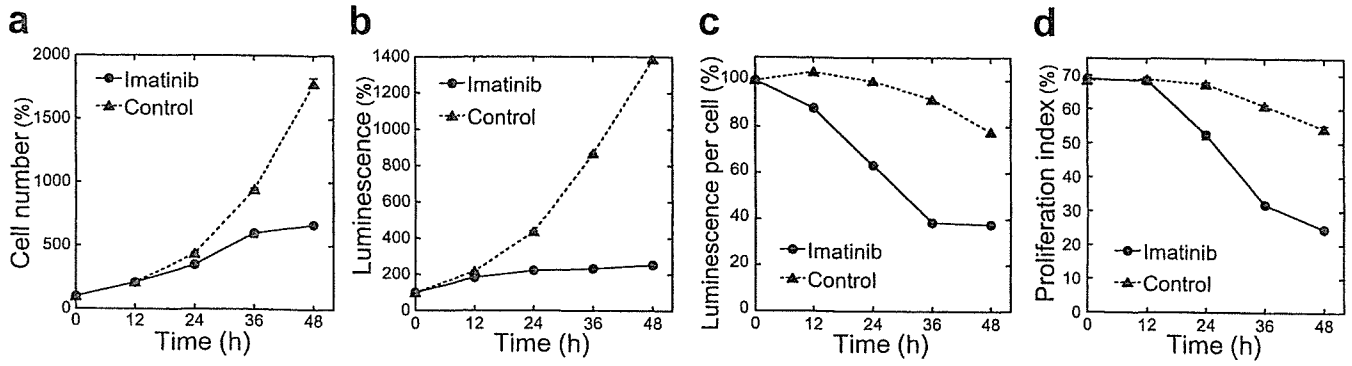

Fig. 6. Sequential assessments of Ba/F3-Luc/Wt cell proliferation in the presence or absence of 1 μ*M* imatinib. Twelve hours after seeding the cells (2×10^4 cells) in 980-μl of medium in a 24-well plate, 20 μl of medium with or without imatinib was added. The measurements were performed immediately after the addition of the medium and every 12 h thereafter. The viable cell numbers (**a**) and luminescence in the standard luciferase assay (**b**) are expressed as percentages of the values at time 0. Imatinib inhibited the increase in cell number and, earlier and more severely, the increase in luciferase activity. Gradual reductions in luminescence per cell (**c**) and proliferative fraction (**d**) are apparent in the presence of imatinib. *Error bars* in panels **a**, **b** and **d** represent standard errors

bioluminescent evaluation of therapies in leukaemia model animal, whereas the feasibility of in vivo monitoring of disease progression and therapeutic response using the cells and bioluminescence imaging needs to be examined in future animal experiments.

Light emission from a tumour, as measured in bioluminescence imaging, is used as a quantitative marker of tumour burden [1, 2]. Proportionality between total luciferase activity of the tumour and the number of viable tumour cells, i.e. constancy of luciferase activity per viable cell, is desirable for such assessment. Previous cell culture studies demonstrated that viable cell numbers correlated linearly with light output in a dilution series of luciferase-expressing cells [3–7], and proportionality was confirmed in the present study for both the standard and intact-cell luciferase assays. However, for a dilution series, the cell conditions are uniform and the potential variations in luciferase expression related to changes in the physiological status of the cell are not taken into consideration. We cultured luciferase-expressing cells under various conditions and compared the luciferase activities, measured using the standard luciferase assay, with the viable cell numbers. In most cases, the time- and dose-dependent patterns for the luciferase activities were similar to those for the viable cell numbers, which suggests that changes in luciferase activity generally reflect changes in viable cell number. However, the luciferase activity per viable cell varied significantly according to the mIL-3 concentration for the factor-dependent cells, and according to the stage of proliferation and imatinib concentration for the factor-independent cells, which distorted the proportionality between viable cell number and bioluminescent signal intensity. Cytokines, proliferative stages and therapeutic drugs are suggested to affect luciferase expression, probably due to alterations in the activity of the LTR promoter. The activity of the CMV promoter has been reported to depend on the cell cycle stage and to be high during the S phase [20]. In our study employing the MMLV LTR, the luciferase activity per cell tended to be higher for cell cultures containing a larger fraction of proliferating cells. Although the molecular mechanisms remain to be studied, cytokines and cell culture conditions may have similar effects on proliferative activity and LTR activity. The signal on in vivo bioluminescence imaging may be related not only to viable cell numbers but also to proliferative activity.

Positive correlations between tumour burden and bioluminescent signal have been shown in many in vivo studies [3, 6, 8–19]. However, Scatena et al. described constant bioluminescent signals despite 3.3-fold increase in tumour volume [34]. A similar discrepancy between liver weight and bioluminescence has been demonstrated for hepatic tumour models with no evidence of significant necrosis or fibrosis on histological examinations [7]. While these observations are attributable partly to enhanced absorption of light photons within large tumours, changes in tumour physiology may also be responsible. In the monitoring of proliferation of the factor-independent, luciferase-expressing cells in the present study, the luciferase activity per viable cell decreased gradually, and the standard luciferase assay underestimated the proliferation, especially during the plateau phase. The medium was not changed during the observation period, and poor medium condition resulting from long incubation may have depressed the activity of the LTR promoter. The progression of implanted tumours in living animals can cause dynamic changes in the microenvironment, such as alterations in the blood supply and oxygenation. Such changes may influence the activity of the LTR promoter and, consequently, signal on in vivo bioluminescence imaging. In vivo bioluminescence imaging has been used for the evaluation of the effects of antineoplastic therapies, including imatinib treatment [28], and bioluminescence has also been used for the in vitro assessment of therapeutic response [13, 35, 36]. In studies with imatinib-sensitive cells, the addition of imatinib to the culture medium reduced the luciferase activity per viable cell in a dose-dependent manner. In sequential measurements after exposure to imatinib, inhibition of the increase in luciferase activity occurred earlier and was more severe than that seen in the viable cell numbers, which suggests that luciferase expression declines early after the addition of imatinib owing to a reduction in the activity of the LTR promoter. Residual tumour burden may be underestimated when the therapeutic effect of imatinib is assessed by in vivo bioluminescence imaging. From another viewpoint, the reduction in luciferase activity per cell may be beneficial, since it enables more sensitive detection of the therapeutic effect.

We performed serial assessments of proliferation using the intact-cell luciferase assay as well as the standard luciferase assay. Although the standard luciferase assay appears to accurately evaluate luciferase activity, the signal on in vivo bioluminescence imaging is not dependent solely on luciferase activity. For in vivo imaging, D-luciferin is absorbed through the peritoneum, is delivered by the blood flow and enters the luciferase-expressing cells. D-Luciferin is oxidised by luciferase in the presence of co-factors (oxygen, adenosine triphosphate and magnesium), resulting in light emission. Some of the emitted light photons pass through the tissues and, finally, are detected by the CCD camera. The intensity of the signal measured by in vivo imaging may depend on various factors, such as D-luciferin absorption through the peritoneum, blood flow, cell membrane permeability, the availability of co-factors, intracellular pH and the transparency of overlying tissues, in addition to the amount of luciferase. Among these parameters, the importance of attenuation of emitted light by overlying tissues has been well recognised [4]. It has also been pointed out that cell uptake of D-luciferin is inefficient and may be a limiting factor for in vivo bioluminescence [37]. The intact-cell luciferase assay may be affected by cell membrane permeability and the intracellular environment and appears to simulate in vivo imaging more faithfully than the standard luciferase assay. In the monitoring of cell proliferation, the decrease in luminescence per cell was less prominent for the intact-cell luciferase assay than for the standard assay. Prolonged incubation appears to lower the

pH of the culture medium, thereby reducing the negative charge of D-luciferin added to the medium. The relative preservation of luminescence per cell in the intact-cell luciferase assay may be attributable to enhancement of cell membrane permeability to D-luciferin by the low pH of the medium [38, 39]. Variations in D-luciferin availability due to changes in the tissue microenvironment may influence the intensity of the signal on in vivo bioluminescence imaging. Various changes may occur in association with disease progression and therapeutic responses in living mice and may affect the relationship between bioluminescent signal and tumour burden. The relationship in living mice remains to be investigated under various conditions.

In conclusion, we generated p190 BCR-ABL-transformed Ba/F3 cell lines stably expressing luciferase under the control of a retroviral LTR for in vivo evaluations of treatment strategies for leukaemia. Our cell culture studies indicate that the bioluminescent signal generally reflects cell proliferation and responses to imatinib. However, differences in cell culture conditions and the addition of imatinib alter the levels of luminescence per cell as well as the fraction of proliferating cells. Although in vivo bioluminescence imaging would allow non-invasive monitoring of leukaemia model animals, environmental factors and therapeutic interventions may cause discrepancies between tumour burden and the intensity of bioluminescence in relation to changes in proliferative activity. The association of luciferase expression with proliferative activity may enhance the sensitivity of bioluminescence imaging to therapeutic responses. The relationship between viable cell number and bioluminescence may vary depending on the cell types and promoters, and it is recommended to examine the relationship for each luciferase-expressing cell line.

Acknowledgements. This work was supported, in part, by grants-in-aid for Scientific Research from the Ministry of Education, Culture, Sports, Science and Technology of Japan.

References

1. Edinger M, Cao YA, Hornig YS, Jenkins DE, Verneris MR, Bachmann MH, et al. Advancing animal models of neoplasia through in vivo bioluminescence imaging. Eur J Cancer 2002;38:2128–2136
2. Contag CH, Jenkins D, Contag PR, Negrin RS. Use of reporter genes for optical measurements of neoplastic disease in vivo. Neoplasia 2000;2:41–52
3. Sweeney TJ, Mailander V, Tucker AA, Olomu AB, Zhang W, Cao Y, et al. Visualizing the kinetics of tumor-cell clearance in living animals. Proc Natl Acad Sci USA 1999;96:12044–12049
4. El Hilali N, Rubio N, Martinez-Villacampa M, Blanco J. Combined noninvasive imaging and luminometric quantification of luciferase-labeled human prostate tumors and metastases. Lab Invest 2002;82:1563–1571
5. Tang Y, Shah K, Messerli SM, Snyder E, Breakefield X, Weissleder R. In vivo tracking of neural progenitor cell migration to glioblastomas. Hum Gene Ther 2003;14:1247–1254
6. Jenkins DE, Oei Y, Hornig YS, Yu SF, Dusich J, Purchio T, et al. Bioluminescent imaging (BLI) to improve and refine traditional murine models of tumor growth and metastasis. Clin Exp Metastasis 2003;20:733–744
7. Sarraf-Yazdi S, Mi J, Dewhirst MW, Clary BM. Use of in vivo bioluminescence imaging to predict hepatic tumor burden in mice. J Surg Res 2004;120:249–255
8. Rehemtulla A, Stegman LD, Cardozo SJ, Gupta S, Hall DE, Contag CH, et al. Rapid and quantitative assessment of cancer treatment response using in vivo bioluminescence imaging. Neoplasia 2000;2:491–495
9. Nyati MK, Symon Z, Kievit E, Dornfeld KJ, Rynkiewicz SD, Ross BD, et al. The potential of 5-fluorocytosine/cytosine deaminase enzyme prodrug gene therapy in an intrahepatic colon cancer model. Gene Ther 2002;9:844–849
10. Vooijs M, Jonkers J, Lyons S, Berns A. Noninvasive imaging of spontaneous retinoblastoma pathway-dependent tumors in mice. Cancer Res 2002;62:1862–1867
11. Shah K, Tang Y, Breakefield X, Weissleder R. Real-time imaging of TRAIL-induced apoptosis of glioma tumors in vivo. Oncogene 2003;22:6865–6872
12. Edinger M, Cao YA, Verneris MR, Bachmann MH, Contag CH, Negrin RS. Revealing lymphoma growth and the efficacy of immune cell therapies using in vivo bioluminescence imaging. Blood 2003;101:640–648
13. Caceres G, Zankina R, Zhu X, Jiao JA, Wong H, Aller A, et al. Determination of chemotherapeutic activity in vivo by luminescent imaging of luciferase-transfected human tumors. Anticancer Drugs 2003;14:569–574
14. Rubin JB, Kung AL, Klein RS, Chan JA, Sun Y, Schmidt K, et al. A small-molecule antagonist of CXCR4 inhibits intracranial growth of primary brain tumors. Proc Natl Acad Sci USA 2003;100:13513–13518
15. Choy G, O'Connor S, Diehn FE, Costouros N, Alexander HR, Choyke P, et al. Comparison of noninvasive fluorescent and bioluminescent small animal optical imaging. Biotechniques 2003;35:1022–6, 1028–1030
16. Smakman N, Martens A, Kranenburg O, Borel Rinkes IH. Validation of bioluminescence imaging of colorectal liver metastases in the mouse. J Surg Res 2004;122:225–230
17. Paroo Z, Bollinger RA, Braasch DA, Richer E, Corey DR, Antich PP, et al. Validating bioluminescence imaging as a high-throughput, quantitative modality for assessing tumor burden. Mol Imaging 2004;3:117–124
18. Nogawa M, Yuasa T, Kimura S, Kuroda J, Sato K, Segawa H, et al. Monitoring luciferase-labeled cancer cell growth and metastasis in different in vivo models. Cancer Lett 2005;217:243–253
19. Shah K, Bureau E, Kim DE, Yang K, Tang Y, Weissleder R, et al. Glioma therapy and real-time imaging of neural precursor cell migration and tumor regression. Ann Neurol 2005;57:34–41
20. Brightwell G, Poirier V, Cole E, Ivins S, Brown KW. Serum-dependent and cell cycle-dependent expression from a cytomegalovirus-based mammalian expression vector. Gene 1997;194:115–123
21. Dong D, Dubeau L, Bading J, Nguyen K, Luna M, Yu H, et al. Spontaneous and controllable activation of suicide gene expression driven by the stress-inducible grp78 promoter resulting in eradication of sizable human tumors. Hum Gene Ther 2004;15:553–561
22. Pane F, Intrieri M, Quintarelli C, Izzo B, Muccioli GC, Salvatore F. BCR/ABL genes and leukemic phenotype: from molecular mechanisms to clinical correlations. Oncogene 2002;21:8652–8667
23. Copelan EA, McGuire EA. The biology and treatment of acute lymphoblastic leukemia in adults. Blood 1995;85:1151–1168

24. Arico M, Valsecchi MG, Camitta B, Schrappe M, Chessells J, Baruchel A, et al. Outcome of treatment in children with Philadelphia chromosome-positive acute lymphoblastic leukemia. N Engl J Med 2000;342:998–1006
25. Gleissner B, Gokbuget N, Bartram CR, Janssen B, Rieder H, Janssen JW, et al. German Multicenter Trials of Adult Acute Lymphoblastic Leukemia Study Group. Leading prognostic relevance of the BCR-ABL translocation in adult acute B-lineage lymphoblastic leukemia: a prospective study of the German Multicenter Trial Group and confirmed polymerase chain reaction analysis. Blood 2002;99:1536–1543
26. Druker BJ, Sawyers CL, Kantarjian H, Resta DJ, Reese SF, Ford JM, et al. Activity of a specific inhibitor of the BCR-ABL tyrosine kinase in the blast crisis of chronic myeloid leukemia and acute lymphoblastic leukemia with the Philadelphia chromosome. N Engl J Med 2001;344:1038–1042
27. Ottmann OG, Druker BJ, Sawyers CL, Goldman JM, Reiffers J, Silver RT, et al. A phase 2 study of imatinib in patients with relapsed or refractory Philadelphia chromosome-positive acute lymphoid leukemias. Blood 2002;100:1965–1971
28. Shah NP, Tran C, Lee FY, Chen P, Norris D, Sawyers CL. Overriding imatinib resistance with a novel ABL kinase inhibitor. Science 2004;305:399–401
29. Palacios R, Steinmetz M. Il-3-dependent mouse clones that express B-220 surface antigen, contain Ig genes in germ-line configuration, and generate B lymphocytes in vivo. Cell 1985;41:727–734
30. Li S, Ilaria RL Jr, Million RP, Daley GQ, Van Etten RA. The P190, P210, and P230 forms of the BCR/ABL oncogene induce a similar chronic myeloid leukemia-like syndrome in mice but have different lymphoid leukemogenic activity. J Exp Med 1999;189:1399–1412
31. Morita S, Kojima T, Kitamura T. Plat-E: an efficient and stable system for transient packaging of retroviruses. Gene Ther 2000;7:1063–1066
32. Kitamura T, Koshino Y, Shibata F, Oki T, Nakajima H, Nosaka T, et al. Retrovirus-mediated gene transfer and expression cloning: powerful tools in functional genomics. Exp Hematol 2003;31:1007–1014
33. von Bubnoff N, Peschel C, Duyster J. Resistance of Philadelphia-chromosome positive leukemia towards the kinase inhibitor imatinib (STI571, Glivec): a targeted oncoprotein strikes back. Leukemia 2003;17:829–838
34. Scatena CD, Hepner MA, Oei YA, Dusich JM, Yu SF, Purchio T, et al. Imaging of bioluminescent LNCaP-luc-M6 tumors: a new animal model for the study of metastatic human prostate cancer. Prostate 2004;59:292–303
35. Qiu Z, Harms JS, Zhu J, Splitter GA. Bovine herpesvirus tegument protein VP22 enhances thymidine kinase/ganciclovir suicide gene therapy for neuroblastomas compared to herpes simplex virus VP22. J Virol 2004;78:4224–4233
36. Mandl SJ, Mari C, Edinger M, Negrin RS, Tait JF, Contag CH, et al. Multi-modality imaging identifies key times for annexin V imaging as an early predictor of therapeutic outcome. Mol Imaging 2004;3:1–8
37. Lee KH, Byun SS, Paik JY, Lee SY, Song SH, Choe YS, et al. Cell uptake and tissue distribution of radioiodine labelled D-luciferin: implications for luciferase based gene imaging. Nucl Med Commun 2003;24:1003–1009
38. Kobatake E, Niimi T, Haruyama T, Ikariyama Y, Aizawa M. Biosensing of benzene derivatives in the environment by luminescent *Escherichia coli*. Biosens Bioelectron 1995; 10:601–605
39. Wood KV, DeLuca M. Photographic detection of luminescence in *Escherichia coli* containing the gene for firefly luciferase. Anal Biochem 1987;1:501–507

International Journal of
HEMATOLOGY

Case Report

Early-Onset Thyrotoxicosis after Unrelated Cord Blood Transplantation for Acute Myelogenous Leukemia

Takaaki Konuma,[a] Akira Tomonari,[a] Satoshi Takahashi,[a] Jun Ooi,[a] Nobuhiro Tsukada,[a] Toshiki Yamada,[a] Hiroyuki Sato,[a] Hitomi Nagayama,[a] Tohru Iseki,[a] Arinobu Tojo,[a] Shigetaka Asano[a,b]

[a]*Department of Hematology/Oncology, The Institute of Medical Science, The University of Tokyo;*
[b]*Integrative Bioscience & Biomedical Engineering, School of Science & Engineering, Waseda University, Tokyo, Japan*

Received November 11, 2005; received in revised form December 20, 2005; accepted December 27, 2005

Abstract

Thyroid dysfunction is a common complication after allogeneic hematopoietic stem cell transplantation (SCT). However, thyrotoxicosis as defined by elevated serum-free thyroxine (FT_4) or free triiodothyronine (FT_3) levels together with low thyroid-stimulating hormone (TSH) levels is rare after SCT. Here we describe 2 patients who developed thyrotoxicosis within the first 50 days after unrelated cord blood transplantation (CBT). Patient 1 is a 32-year-old woman with acute myelogenous leukemia (AML)-M5a who underwent CBT. On day +41, she developed tachycardia. On day +48, FT_4 increased to 2.2 ng/dL and TSH was suppressed to less than 0.1 μU/mL. Antithyroid peroxidase antibody was positive. On day +83, FT_4 spontaneously decreased to 1.4 ng/dL. Patient 2 is a 42-year-old man with AML-M4 who underwent CBT. On day +42, he developed tachycardia. On day +48, FT_3 increased to 4.75 pg/mL and TSH was suppressed to 0.02 μU/mL. Antithyroid peroxidase antibody was positive. Eight months after CBT, his thyroid function spontaneously returned to normal. The presence of antithyroid peroxidase antibody suggested that immune-mediated reactions might be associated with the development of thyrotoxicosis after CBT in our patients. The present study shows that thyrotoxicosis can occur during very early periods after CBT.
Int J Hematol. 2006;83:348-350. doi: 10.1532/IJH97.05166

Key words: Thyrotoxicosis; AML; Cord blood; Transplantation; Autoimmune

1. Introduction

Thyroid dysfunction is one of the common complications after allogeneic hematopoietic stem cell transplantation (SCT). Overt or compensated hypothyroidism usually occurs as a late complication of SCT [1]. The use of total body irradiation (TBI) in a conditioning regimen has been considered to be mainly responsible for the occurrence of late-onset hypothyroidism [2]. Within the first 6 months after SCT, the most common thyroid dysfunction is euthyroid sick syndrome (ESS), defined by decreased serum-free triiodothyronine (FT_3) and/or free thyroxine (FT_4) levels together with normal or low thyroid-stimulating hormone (TSH) levels [3,4]. Previous studies reported that 43% to 48% of patients who underwent bone marrow transplantation (BMT) with or without the use of TBI developed ESS at 3 months after BMT. In contrast, thyrotoxicosis as defined by elevated serum FT_3 or FT_4 levels together with low TSH levels is rare after SCT. Recently, Kami et al reported that 7 (12%) of 57 patients developed thyrotoxicosis within 6 months after BMT [5]. The onset of thyrotoxicosis ranged from 61 to 176 days after BMT. In this study, we describe 2 patients who developed thyrotoxicosis within the first 50 days after umbilical cord blood transplantation (CBT).

Correspondence and reprint requests: Akira Tomonari, MD, PhD, Department of Hematology/Oncology, The Institute of Medical Science, The University of Tokyo, 4-6-1, Shirokanedai, Minato-ku, Tokyo 108-8639, Japan; 81-3-3443-8111; fax: 81-3-5449-5429 (e-mail: atomonar@ims.u-tokyo.ac.jp).

2. Case Report

Patient 1 is a 32-year-old woman with acute myelogenous leukemia (AML)-M5a who achieved complete remission (CR) after 3 courses of chemotherapy. Thyroid function tests before CBT were normal, showing serum FT_4 of 1.1 ng/dL (normal range, 0.9-1.8 ng/dL) and TSH of 2.4 μU/mL (normal range, 0.6-4.9 μU/mL). Antithyroid microsomal and antithyroglobulin antibodies were negative. She underwent CBT following a conditioning regimen with 12 Gy TBI, 120 mg/kg cyclophosphamide, and 12 g/m^2 cytarabine with granulocyte colony-stimulating factor (G-CSF) in September

2000 [6,7]. The cord blood (CB) grafts contained 5.29 × 10^7/kg total nucleated cells from an unrelated donor with 1 locus-mismatch in HLA-DR. Graft-versus-host disease (GVHD) prophylaxis consisted of cyclosporine and a short course of methotrexate. A neutrophil count consistently greater than 500/μL was achieved on day +28. Grade II acute GVHD involving the skin occurred, but resolved without steroid therapy. Cytomegalovirus infection was not documented by an antigenemia assay. On day +41, she developed tachycardia with a heart rate (HR) ranging from 100 to 140 beats/minute at rest. She had no fever. Physical examination did not reveal any other abnormalities. The thyroid gland was painless and not enlarged. Thyroid function tests on day +48 showed an elevated FT_4 level of 2.2 ng/dL and a suppressed TSH level of less than 0.1 μU/mL. She received a diagnosis of thyrotoxicosis. Because the symptoms were mild, no treatments were administered. Her HR at rest tended to decrease to between 90 and 120 beats/minute on day +52, and further decreased to less than 90 beats/minute on day +62. Antithyroid peroxidase antibody was positive with a level of 2.2 U/mL (normal level, < 0.3 U/mL) on day +62. Antithyroid microsomal, antithyroglobulin, and antithyroid receptor antibodies were negative. On day +83, FT_4 decreased to 1.4 ng/dL, but TSH was still suppressed to less than 0.1 μU/mL. Leukemia relapsed 14 months after CBT, and she died 8 months later.

Patient 2 is a 42-year-old man with AML-M4 who failed to achieve CR after 4 courses of chemotherapy. Thyroid function tests before CBT were normal showing FT_4 of 1.26 ng/dL (normal range, 0.95-1.74 ng/dL) and TSH of 0.57 μU/mL (normal range, 0.38-3.64 μU/mL). Antithyroid microsomal and antithyroglobulin antibodies were negative. He underwent CBT in May 2003. The conditioning regimen and GVHD prophylaxis were the same as for Patient 1. The CB grafts contained 3.05 × 10^7/kg total nucleated cells from 2 unrelated donors both with 2 locus-mismatches in HLA-B and DR. A neutrophil count consistently greater than 500/μL was achieved on day +25. On day +28, full donor chimerism from 1 of 2 donors was confirmed in bone marrow cells. Grade II acute GVHD involving the skin occurred, but resolved without steroid therapy. He developed positive cytomegalovirus antigenemia and received ganciclovir therapy on day +36. From day +42, he developed tachycardia with HR ranging from 100 to 130 beats/minute at rest. He had no fever. Physical examination did not reveal any other abnormalities. The thyroid gland was painless and not enlarged. On day +48, serum FT_4 and FT_3 levels increased to 1.69 ng/dL and 4.75 pg/mL (normal range, 2.13-4.07 pg/mL), respectively, and the TSH level was suppressed to 0.02 μU/mL. He received a diagnosis of thyrotoxicosis, which was not treated. His HR at rest tended to decrease to between 80 and 110 beats/minute on day +50, and further decreased to less than 80 beats/minute from day +71. Antithyroid peroxidase antibody was positive with a level of 1.81 U/mL on day +61. Antithyroid microsomal, antithyroglobulin, and antithyroid receptor antibodies were negative. On day +76, FT_4 and FT_3 tended to decrease to 1.21 ng/dL and 4.26 pg/mL, respectively, and TSH tended to increase to 0.08 μU/mL. Eight months after CBT, thyroid function tests returned to normal, showing FT_4 of 1.39 ng/dL, FT_3 of 3.71 pg/mL, and TSH of 0.88 μU/mL. However, leukemia relapsed 8 months after CBT, and he died 7 months later.

3. Discussion

Thyrotoxicosis is a rare complication after SCT. We presented here 2 patients who developed thyrotoxicosis after CBT. This is the first report of thyrotoxicosis occurring after CBT. The severity of thyrotoxicosis in our patients was mild. In addition to the negative feedback mechanism of the pituitary-thyroid axis, low levels of TSH might be attributable to impaired secretion of TSH [8,9]. Compared with thyrotoxicosis after BMT in previous reports, the most distinctive feature of thyrotoxicosis in our patients was that the onset was extremely early after transplantation. In both patients, thyrotoxicosis was diagnosed on day +48.

Kami et al have reported early changes of thyroid function after BMT [5]. They showed that 7 (12%) of 57 patients developed thyrotoxicosis during the first 6 months after BMT. The onset of thyrotoxicosis was a median of 104 days (range, 61-176 days) after BMT. Thyrotoxicosis was transient in all patients. The median duration was 2 months (range, 1-3 months). Six of 7 patients had antithyroid peroxidase antibody, antithyroglobulin antibody, or antithyroid receptor antibody. The mechanisms of thyrotoxicosis developing early after SCT remained unclear. Various factors might contribute to the development of thyrotoxicosis after SCT. These included a conditioning regimen [1,2], GVHD [10], viral infection [11], genetic predisposition [12], and adaptive transfer of autoimmune thyroiditis from the donor [13,14]. However, the presence of antithyroid peroxidase antibody suggested that immune-mediated reactions might be associated with thyrotoxicosis after CBT in our patients.

CB grafts contain fetal lymphocytes. Thus, there may be some similarity between postpartum thyroiditis and thyrotoxicosis after CBT in our patients. In postpartum thyroiditis, transient thyrotoxicosis generally occurs 1 to 3 months after delivery and lasts for 1 to 2 months [15]. The symptoms are often quite mild. Antithyroid peroxidase antibody or antithyroglobulin antibody is found in 52% to 100% of patients. Lymphocytic infiltration of the thyroid gland causes transient thyrotoxicosis. Recently, the presence of fetal cells in the maternal thyroid gland has been identified [16]. Intrathyroidal fetal microchimerism is considered to play a role in the occurrence of postpartum autoimmune thyroid disease [17]. To identify the pathogenesis of thyrotoxicosis after CBT, histological examination of the thyroid is necessary.

Between August 1998 and January 2005, 86 adults underwent CBT using a conditioning regimen, including 12 Gy TBI in our institution. Among them, only 2 patients were diagnosed with thyrotoxicosis after CBT. This might be an underestimation of the true incidence rate, because the thyroid function was not evaluated in all CBT patients. Prospective large-scale studies are needed to determine the incidence, clinical features, and risk factors for thyrotoxicosis after CBT. This study shows that thyrotoxicosis can occur during very early periods after CBT.

Acknowledgments

The authors thank Maki Monna-Oiwa for her secretarial assistance. We also thank the Kobayashi Foundation for financial support.

References

1. Sanders JE. Growth and development after hematopoietic cell transplantation. In: Blume KG, Forman SJ, Appelbaum FR, eds. *Thomas' Hematopoietic Cell Transplantation.* 3rd ed. Oxford: Blackwell Scientific Publications; 2004:929-943.
2. Boulad F, Bromley M, Black P, et al. Thyroid dysfunction following bone marrow transplantation using hyperfractionated radiation. *Bone Marrow Transplant.* 1995;15:71-76.
3. Vexiau P, Perez-Castiglioni P, Socie G, et al. The 'euthyroid sick syndrome': incidence, risk factors and prognostic value soon after allogeneic bone marrow transplantation. *Br J Haematol.* 1993;85: 778-782.
4. Toubert ME, Socie G, Gluckman E, et al. Short- and long-term follow-up of thyroid dysfunction after allogeneic bone marrow transplantation without the use of preparative total body irradiation. *Br J Haematol.* 1997;98:453-457.
5. Kami M, Tanaka Y, Chiba S, et al. Thyroid function after bone marrow transplantation: possible association between immune-mediated thyrotoxicosis and hypothyroidism. *Transplantation.* 2001;71: 406-411.
6. Ooi J, Iseki T, Takahashi S, et al. Unrelated cord blood transplantation for adult patients with de novo acute myeloid leukemia. *Blood.* 2004;103:489-491.
7. Takahashi S, Iseki T, Ooi J, et al. Single-institute comparative analysis of unrelated bone marrow transplantation and cord blood transplantation for adult patients with hematologic malignancies. *Blood.* 2004;104:3813-3820.
8. Wehmann RE, Gregerman RI, Burns WH, Saral R, Santos GW. Suppression of thyrotropin in the low-thyroxine state of severe nonthyroidal illness. *N Engl J Med.* 1985;312:546-552.
9. Hershman JM, Eriksen E, Kaufman N, Champlin RE. Thyroid function tests in patients undergoing bone marrow transplantation. *Bone Marrow Transplant.* 1990;6:49-51.
10. Mulligan SP, Joshua DE, Joasoo A, Kronenberg H. Autoimmune hyperthyroidism associated with chronic graft-versus-host disease. *Transplantation.* 1987;44:463-464.
11. Kawano C, Muroi K, Akioka T, Izumi T, Kodera Y, Ozawa K. Cytomegalovirus pneumonitis, activated prothrombin time prolongation and subacute thyroiditis after unrelated allogeneic bone marrow transplantation. *Bone Marrow Transplant.* 2000;26: 1347-1349.
12. Au WY, Hawkins BR, Chan EY, et al. Association of the HLA A2-B46-DR9 haplotype with autoimmune thyroid dysfunction after bone marrow transplantation in Chinese patients. *Br J Haematol.* 2001;115:660-663.
13. Aldouri MA, Ruggier R, Epstein O, Prentice HG. Adoptive transfer of hyperthyroidism and autoimmune thyroiditis following allogeneic bone marrow transplantation for chronic myeloid leukaemia. *Br J Haematol.* 1990;74:118-119.
14. Ichihashi T, Yoshida H, Kiyoi H, et al. Development of hyperthyroidism in donor and recipient after allogeneic bone marrow transplantation. *Bone Marrow Transplant.* 1992;10:397-398.
15. Roti E, Emerson CH. Clinical review 29: postpartum thyroiditis. *J Clin Endocrinol Metab.* 1992;74:3-5.
16. Ando T, Davies TF. Clinical review 160: postpartum autoimmune thyroid disease: the potential role of fetal microchimerism. *J Clin Endocrinol Metab.* 2003;88:2965-2971.
17. Renne C, Ramos Lopez E, Steimle-Grauer SA, et al. Thyroid fetal male microchimerisms in mothers with thyroid disorders: presence of Y-chromosomal immunofluorescence in thyroid-infiltrating lymphocytes is more prevalent in Hashimoto's thyroiditis and Graves' disease than in follicular adenomas. *J Clin Endocrinol Metab.* 2004; 89:5810-5814.

Molecular Imaging • Vol. 5, No. 2, April–June 2006, pp. 53–56

Light Emission Requires Exposure to the Atmosphere in Ex Vivo Bioluminescence Imaging

Yusuke Inoue, Kiyoko Izawa, Arinobu Tojo, Rieko Sekine, Toshiyuki Okubo, and Kuni Ohtomo

University of Tokyo, Japan

Abstract

The identification of organs bearing luciferase activity by in vivo bioluminescence imaging (BLI) is often difficult, and ex vivo imaging of excised organs plays a complementary role. This study investigated the importance of exposure to the atmosphere in ex vivo BLI. Mice were inoculated with murine pro-B cell line Ba/F3 transduced with firefly luciferase and p190 BCR-ABL. They were killed following in vivo BLI, and whole-body imaging was done after death and then after intraperitoneal air injection. In addition, the right knee was exposed and imaged before and after the adjacent bones were cut. Extensive light signals were seen on in vivo imaging. The luminescence disappeared after the animal was killed, and air injection restored the light emission from the abdomen only, suggesting a critical role of atmospheric oxygen in luminescence after death. Although no substantial light signal at the right knee was seen before bone cutting, light emission was evident after cutting. In conclusion, in ex vivo BLI, light emission requires exposure to the atmosphere. Bone destruction is required to demonstrate luciferase activity in the bone marrow after death. *Mol Imaging* (2006) 5, 53–56.

Keywords: Bioluminescence imaging, luciferase, ex vivo method, oxygen, bone marrow.

Introduction

In vivo bioluminescence imaging (BLI) enables one to evaluate the intensity and distribution of expression of the luciferase gene in an intact laboratory animal and is used increasingly for various purposes, such as monitoring gene therapy and cell trafficking, investigating transcriptional regulation, and evaluating protein–protein interactions [1]. Commonly, animals expressing firefly luciferase are injected with D-luciferin for in vivo BLI. Light photons are produced through the oxidation of D-luciferin in the presence of oxygen, adenosine triphosphate, and magnesium [2] and are detected by using a sensitive charge-coupled device (CCD) camera. Whole-body, quantitative assessments of luciferase expression can be performed repetitively in a given animal.

Bioluminescence imaging provides projectional images, not tomographic images, and, in addition, the scattering of light photons impairs the spatial resolution. These factors reduce the ability of in vivo BLI to identify the organs with luciferase activity. Using a CCD camera, one can easily determine the luciferase-expressing organs by imaging the excised organs after D-luciferin injection, an imaging procedure called ex vivo BLI [3–8]. Ex vivo imaging enhances the detectability of luciferase expression [7,9], and the quantitative accuracy of ex vivo imaging has been validated by using a conventional luciferase assay of organ homogenates as a standard [3]. Although ex vivo imaging is invasive and does not allow repetitive assessments of an individual animal, it serves as a valuable adjunct to in vivo imaging for detailed evaluation.

It has been reported that the luminescence of the liver of a mouse having luciferase-expressing intrahepatic tumors and hemorrhagic ascites disappeared after sacrifice and recovered after excision of the liver [10]. The authors attributed the increase in the light signal after excision to the increased oxygen availability on exposure to ambient air. However, light photons are severely attenuated by the tissues and blood, and the increase in the detected light signal might be due to the elimination of attenuation by the abdominal wall and hemorrhagic ascites. In this study, we investigated the importance of exposure to the atmosphere in ex vivo BLI to obtain insight into the ex vivo technique.

Materials and Methods

Cell Lines

The interleukin-3 (IL-3)-dependent murine pro-B cell line Ba/F3 was transfected with both the firefly luciferase gene and the wild-type p190 BCR-ABL fusion gene retrovirally as described previously [11], and the established cells were termed Ba/F3-Luc/Wt cells. The cDNA encoding the firefly luciferase was excised from the pGL3-basic vector (Promega, Madison, WI), and the

Abbreviations: BLI, bioluminescence imaging; CCD, charge-coupled device; IL-3, interleukin-3; ALL, acute lymphoblastic leukemia.

Corresponding author: Yusuke Inoue, Department of Radiology, Institute of Medical Science, University of Tokyo, 4-6-1 Shirokanedai, Minato-ku, Tokyo 108-8639, Japan; e-mail: inoueys-tky@umin.ac.jp.

Received 11 January 2006; Received in revised form 28 February 2006; Accepted 7 March 2006.
DOI 10.2310/7290.2006.00015

long-term stability of luciferase expression in the established cells was confirmed in vitro. The p190 BCR-ABL fusion gene is important in the development of acute lymphoblastic leukemia (ALL) [12], and Ba/F3 cells transformed with p190 BCR-ABL show IL-3-independent, autonomous proliferation [13]. The Ba/F3-Luc/Wt cells were maintained in RPMI 1640 medium (Invitrogen, Grand Island, NY) supplemented with 10% (v/v) fetal bovine serum (FBS, JRH Biosciences, Lenexa, KS) and 1% penicillin/streptomycin (Invitrogen), in the absence of IL-3. Cultures were incubated at 37 C in 5% CO_2.

Animals

Five 8-week-old female BALB/c nu/nu mice were inoculated with 2 10^6 Ba/F3-Luc/Wt cells intravenously via the tail vein. The mice were obtained from SLC Japan (Tokyo, Japan) and were handled according to the guidelines of the Institute of Medical Science, University of Tokyo. The experiments were approved by the committee for animal research at the institution.

Imaging Procedures

About 4 weeks after cell inoculation, we performed BLI with a cooled CCD camera system (IVIS Imaging System 100, Xenogen, Alameda, CA). The mice received an intraperitoneal injection of 150 mg/kg D-luciferin, and photographic and luminescent images in the dorsal, left lateral, ventral, and right lateral projections were acquired under isoflurane anesthesia (in vivo BLI). Additional ventral images were obtained 20 min after injection. Subsequently, the mice were killed by cervical dislocation and then imaged repetitively. About 10 min after death, 4 mL of air was injected intraperitoneally, and imaging was performed again. The imaging parameters used to acquire these whole-body luminescent images were an exposure time of 10 sec and binning of 8. A region of interest covering the entire mouse except the tail was placed on the ventral image, and the whole-body signal intensity was quantified by using the Living Image software (version 2.50, Xenogen).

Following the whole-body imaging, ex vivo imaging of the excised organs was performed. The liver, spleen, intestine, ovary, uterus, kidney, lung, and heart were imaged using the CCD camera system. In addition, the right knee was exposed, and ventral images of the body remaining after removing the internal organs were obtained. The imaging was repeated after cutting the right distal femur and right proximal tibia. A region of interest was placed over the right knee, and the signal intensity was compared before and after cutting. The imaging parameters used to obtain the ex vivo luminescent images were an exposure time of 10 sec and binning of 4 or 8.

Results

In vivo BLI demonstrated extensive light signals, indicating proliferation of the implanted cells in various regions, including the head and neck, chest, abdomen, and limbs (Figure 1). After sacrifice, the light signal decreased rapidly and essentially disappeared within several minutes. The whole-body signal intensities in the ventral projection just before sacrifice, 2 min after death, and 5 min after death were 3.49 $10^8 \pm 9.10$ 10^7 (mean $\pm$ *SD*), 1.43 $10^6 \pm 7.28$ 10^5, and 2.25 $10^5 \pm 1.06$ 10^5 p s $^{-1}$, respectively. Intraperitoneal air injection definitely increased the signal (6.62 $10^7 \pm$ 2.65 10^7 p s $^{-1}$ 5 min after injection), while the light sources were localized only in the abdomen.

Ex vivo imaging of the excised organs showed intense light signals for the liver and spleen. Signals were also observed for the lung, intestine, and gynecologic organs, except for the absence of intestinal signals in one mouse. Imaging of the body remaining after removal of the internal organs showed a small bright focus in the paraaortic region in two mice. Enlarged paraaortic lymph nodes were removed and imaged together with the remaining body, and the lymph nodes were proven to be the light sources. In two mice, light emission from the anterior thorax near the thoracotomy incision was shown. For the right knee, no substantial luminescent signal was found before bone cutting. The light signal increased dramatically after bone cutting (Figure 2). The signal intensities for the right knee before and 1 min

Figure 1. *Whole-body bioluminescence images. The pseudocolor luminescent image is overlaid on the grayscale photographic image. Shown are ventral images before sacrifice (left), 5 min after death (middle), and 5 min after intraperitoneal air injection (right). The same color scale was used in the three panels. The light signal disappeared after death and was recovered only for the abdomen after air injection.*

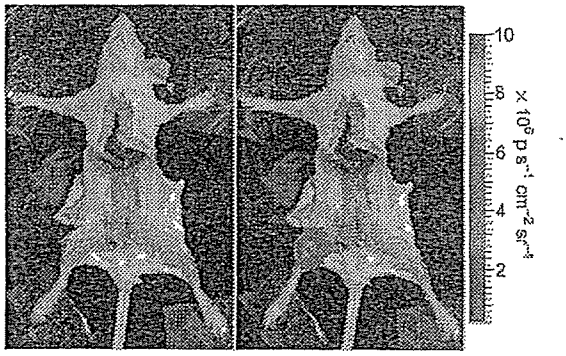

Figure 2. *Bioluminescence images before (left) and 1 min after (right) cutting around the right knee. The same color scale was used for both panels. A light signal at the right knee was seen only after cutting.*

after cutting were 1.72 $10^5 \pm 5.75$ 10^4 and 3.51 $10^7 \pm 2.66$ 10^7 p s ^{1}, respectively.

Discussion

Patients with Philadelphia chromosome-positive ALL frequently express the p190 BCR-ABL fusion protein and have a poor prognosis [12]. Although the BCR-ABL tyrosine kinase inhibitor, imatinib mesylate (Novartis Pharmaceuticals, Basel, Switzerland), is effective, resistance to this drug develops rapidly and novel therapeutic strategies need to be explored [14]. Ba/F3-Luc/Wt cells show IL-3-independent, autonomous proliferation and stable luciferase expression, and mice injected with the cells intravenously may be used to evaluate treatments for Philadelphia chromosome-positive ALL by in vivo BLI.

The mice implanted with Ba/F3-Luc/Wt cells showed extensive light emission in vivo. This light signal disappeared after death, as described previously [10], and the intraperitoneal air injection restored light emission from the abdomen only. Light photons should be attenuated similarly before and after air injection, and these observations support the hypothesis that luminescence after sacrifice requires exposure to the atmosphere. Luminescence from cells transduced with firefly luciferase relies on the oxidation of D-luciferin catalyzed by luciferase. Oxygen in the atmosphere appears to play a critical role in the oxidation after death.

Although the identification of the involved organs was difficult from in vivo images, ex vivo imaging showed the proliferation of implanted cells in the liver, spleen, lung, intestine, gynecologic organs, and lymph nodes. However, signals from these organs could not fully explain those observed on in vivo images. Proliferation in the bone marrow is expected based on the nature of Ba/F3 cells. Although some in vivo signals appeared to originate from the skeletal system, light signals were essentially absent on imaging the remaining body after removing the internal organs and involved lymph nodes, except for the signal from the anterior thorax near the thoracotomy incision in two mice. We evaluated luminescence at the right knee further. Whereas in vivo BLI suggested luminescence at the site, imaging of the dead body did not show a substantial light signal, even after removal of the overlying tissues. Subsequent cutting around the knee restored the light emission dramatically. The transfer of oxygen from the atmosphere to cells within the bone marrow cavity appeared to be blocked by the bone cortex. The signal from the anterior thorax was probably attributable to luminescence in the incised sternum. Our results indicate that destruction of the bone cortex is required to assess luciferase expression in the bone marrow.

Although the need for oxygen in luciferase reaction is well known, to the best of our knowledge, the crucial role of exposure to atmospheric oxygen in ex vivo imaging has not been clearly demonstrated. In particular, the knowledge that bone destruction is required to assess luciferase activity in the bone marrow would be important in experiments using models of bone metastasis and blood cell transplantation. If a researcher picks up a bone, taking care not to damage the bone, and image it, he or she may miss luciferase activity in the bone marrow cavity. If a researcher does not know the need for bone destruction, he or she may image the whole skeleton after removing skin and soft tissues to assess luciferase activity in the bone marrow, resulting in failure of detection.

In summary, we demonstrated that light emission in ex vivo BLI needs exposure to the atmosphere. Researchers should be aware that bone destruction is required to elucidate luciferase activity in the bone marrow cavity after sacrifice.

Acknowledgments

This work was supported in part by Grants-in-Aid for Scientific Research from the Ministry of Education, Culture, Sports, Science and Technology of Japan.

References

[1] Contag CH, Ross BD (2002). It's not just about anatomy: In vivo bioluminescence imaging as an eyepiece into biology. *J Magn Reson Imaging.* **16**:378–387.

[2] Day JC, Tisi LC, Bailey MJ (2004). Evolution of beetle bioluminescence: The origin of beetle luciferin. *Luminescence.* **19**:8–20.

[3] Carlsen H, Moskaug JO, Fromm SH, Blomhoff R (2002). In vivo imaging of NF-kappa B activity. *J Immunol.* **168**:1441–1446.

[4] Yull FE, Han W, Jansen ED, Everhart MB, Sadikot RT, Christman JW, Blackwell TS (2003). Bioluminescent detection of endotoxin effects on HIV-1 LTR-driven transcription in vivo. *J Histochem Cytochem.* **51**:741–749.

[5] Kalikin LM, Schneider A, Thakur MA, Fridman Y, Griffin LB, Dunn RL, Rosol TJ, Shah RB, Rehemtulla A, McCauley LK, Pienta KJ (2003). In vivo visualization of metastatic prostate cancer and quantitation of disease progression in immunocompromised mice. *Cancer Biol Ther.* **2**:656–660.

[6] Jenkins DE, Yu SF, Hornig YS, Purchio T, Contag PR (2003). In vivo monitoring of tumor relapse and metastasis using bioluminescent PC-3M-luc-C6 cells in murine models of human prostate cancer. *Clin Exp Metastasis.* **20**:745–756.

[7] Jenkins DE, Oei Y, Hornig YS, Yu SF, Dusich J, Purchio T, Contag PR (2003). Bioluminescent imaging (BLI) to improve and refine traditional murine models of tumor growth and metastasis. *Clin Exp Metastasis.* **20**:733–744.

[8] Liang Q, Yamamoto M, Curiel DT, Herschman HR (2004). Noninvasive imaging of transcriptionally restricted transgene expression following intratumoral injection of an adenovirus in which the COX-2 promoter drives a reporter gene. *Mol Imaging Biol.* **6**:395–404.

[9] Yoshimitsu M, Sato T, Tao K, Walia JS, Rasaiah VI, Sleep GT, Murray GJ, Poeppl AG, Underwood J, West L, Brady RO, Medin JA (2004). Bioluminescent imaging of a marking transgene and correction of Fabry mice by neonatal injection of recombinant lentiviral vectors. *Proc Natl Acad Sci USA.* **101**:16909–16914.

[10] Sarraf-Yazdi S, Mi J, Dewhirst MW, Clary BM (2004). Use of in vivo bioluminescence imaging to predict hepatic tumor burden in mice. *J Surg Res.* **120**:249–255.

[11] Inoue Y, Tojo A, Sekine R, Soda Y, Kobayashi S, Nomura A, Izawa K, Kitamura T, Okubo T, Ohtomo K (2006 February 24). In vitro validation of bioluminescent monitoring of disease progression and therapeutic response in leukaemia model animals. *Eur J Nucl Med Mol Imaging.* [E-pub ahead of print]

[12] Copelan EA, McGuire EA (1995). The biology and treatment of acute lymphoblastic leukemia in adults. *Blood.* **85**:1151–1168.

[13] Li S, Ilaria RL Jr., Million RP, Daley GQ, Van Etten RA (1999). The P190, P210, and P230 forms of the BCR/ABL oncogene induce a similar chronic myeloid leukemia-like syndrome in mice but have different lymphoid leukemogenic activity. *J Exp Med.* **189**:1399–1412.

[14] Ottmann OG, Druker BJ, Sawyers CL, Goldman JM, Reiffers J, Silver RT, Tura S, Fischer T, Deininger MW, Schiffer CA, Baccarani M, Gratwohl A, Hochhaus A, Hoelzer D, Fernandes-Reese S, Gathmann I, Capdeville R, O'Brien SG (2002). A phase 2 study of imatinib in patients with relapsed or refractory Philadelphia chromosome-positive acute lymphoid leukemias. *Blood.* **100**:1965–1971.

Establishment of Perineural Invasion Models and Analysis of Gene Expression Revealed an Invariant Chain (CD74) as a Possible Molecule Involved in Perineural Invasion in Pancreatic Cancer

Norimasa Koide,[1,5] Taketo Yamada,[1] Rie Shibata,[1] Taisuke Mori,[1] Mariko Fukuma,[1] Ken Yamazaki,[1,3] Koichi Aiura,[2] Motohide Shimazu,[2] Setsuo Hirohashi,[4] Yuji Nimura,[5] and Michiie Sakamoto[1]

Abstract **Purpose:** Perineural invasion causes frequent local recurrence even after resection and a poor prognosis for pancreatic cancer. We established perineural invasion models and analyzed the molecular mechanism of perineural invasion in pancreatic cancer.

Experimental Design: Seven pancreatic cancer cell lines with or without human peripheral nerves were s.c. implanted in nonobese diabetes/severe combined immunodeficient mice. We compared expression profiles among high and low perineural invasion cell lines by using an oligonucleotide microarray. We examined up-regulation of the invariant chain (CD74) in high perineural invasion cell lines in mRNA and protein levels and surgical cases immunohistochemically.

Results: Four of seven pancreatic cancer cell lines (CaPan1, CaPan2, CFPAC, and MPanc96) showed perineural invasion to s.c. transplanted human peripheral nerves. Moreover, CaPan1 and CaPan2 (high perineural invasion group) also resulted in a high frequency of perineural invasion to mouse s.c. peripheral nerves, whereas three pancreatic cancer cell lines HPAFII, AsPC1, and Panc1 (low perineural invasion group) did not show perineural invasion to either human or mouse nerves. We identified 37 up-regulated genes and 12 down-regulated genes in the high perineural invasion group compared with the low perineural invasion group. Among them, CD74 was up-regulated in the high perineural invasion group in mRNA and protein levels. Furthermore, immunohistochemical expression of CD74 in clinical cases revealed its significant overexpression in pancreatic cancer with perineural invasion ($P < 0.008$).

Conclusions: This is the first report of perineural invasion models using human pancreatic cancer cell lines. In combination with gene expression profiling, it was indicated that CD74 could be a candidate molecule involved in perineural invasion. These models provide new approaches for study of perineural invasion in pancreatic cancer.

Pancreatic cancer is the fourth leading cause of cancer-related death in the United States (1). Worldwide pancreatic cancer causes an estimated 213,000 deaths a year (2). In the United States, ~32,180 patients are diagnosed with pancreatic cancer annually, and nearly an equal number will die from the disease (1). When first diagnosed with pancreatic cancer, about 80% of all patients receive palliative therapy instead of surgery because of locally advanced disease, depending on perineural invasion or metastasis. The remaining 20% of patients receiving surgery still have a poor prognosis due to high incidence and early occurrence of local recurrence and hepatic and lymph node metastasis, even after pathologically curative surgery (3–5). It is suspected that microscopic hepatic metastasis is already present (6). Cancer cells spreading in the perineural space even at an early clinical stage also cause local recurrence in the retroperitoneum because of residual tumor cells in the perineural space after surgical resection (7). Moreover, many previous clinicopathologic reports showed that perineural invasion in pancreatic cancer was one of the most significant poor prognostic factors (8, 9).

Genetic alternations seem to be responsible for the development of pancreatic cancer (10). Recently, pancreatic cancer–specific expression profiles using cDNA microarrays (11–13), Affymetrix gene chip (14, 15), and serial analysis of gene expression (16) have been used by many investigators. However, the molecular mechanisms of hepatic metastasis and perineural invasion in pancreatic cancer are far from clear. Some studies reported metastasis-related genes by analyzing gene expression profiles between a highly metastatic variant and a parental pancreatic cancer cell line in an orthotopic

Authors' Affiliations: Departments of [1]Pathology and [2]Surgery, School of Medicine, Keio University; [3]Genomic Division and [4]Pathology Division, National Cancer Center Research Institute, Tokyo, Japan; and [5]Division of Surgical Oncology, Department of Surgery, Nagoya University, Nagoya, Japan

Received 8/23/05; revised 1/12/06; accepted 2/2/06.

Grant support: Grant-in-aid for the 21th Century Center of Excellence program and Cancer Research from the Ministry of Education, Culture, Sports, Science and Technology of Japan, for the Third Term Comprehensive 10-Year Strategy for Cancer Control from the Ministry of Health, Labor and Welfare of Japan, and for Cancer Research from the Foundation for Promotion of Cancer Research.

The costs of publication of this article were defrayed in part by the payment of page charges. This article must therefore be hereby marked *advertisement* in accordance with 18 U.S.C. Section 1734 solely to indicate this fact.

Requests for reprints: Michiie Sakamoto, Department of Pathology, School of Medicine, Keio University, 35 Shinanomachi, Shinjyuku-ku, Tokyo, 160-8582, Japan. Phone: 81-3-5363-3764; Fax: 81-03-3353-3290; E-mail: msakamot@sc.itc.keio.ac.jp.

doi:10.1158/1078-0432.CCR-05-1852

transplanted nude mouse model (17, 18). However, there are few reports about the molecular mechanisms of perineural invasion of pancreatic cancer due to the lack of good disease models. Understanding perineural invasion at the molecular level is an important step towards the identification of prognostic markers and therapeutic targets for pancreatic cancer treatment.

To analyze the mechanisms of perineural invasion in pancreatic cancer, we constructed perineural invasion models using s.c. implantation of human pancreatic cancer cell lines. CaPan1 and CaPan2 (high perineural invasion group) implanted s.c. into nonobese diabetes/severe combined immunodeficient (NOD/SCID) mice were frequently found to form perineural invasion to the mouse s.c. nerves and transplanted human nerves, whereas three pancreatic cancer cell lines HPAFII, AsPC1, and Panc1 (low perineural invasion group) did not show perineural invasion to either human or mouse nerves. Next, we compared gene expression profiles between the high and low perineural invasion groups using a microarray technique. Of these genes, we further investigated whether *invariant chain* (*CD74*) expression was associated with perineural invasion.

Materials and Methods

Cell culture. The human pancreatic cancer cell lines CaPan1, CaPan2, HPAFII, AsPC1, Panc1, CFPAC, and MPanc96 were obtained from the American Type Culture Collection (Manassas, VA). All cell lines were cultured in RPMI 1640 (Sigma, St. Louis, MO) containing 10% heat-inactivated fetal bovine serum, 100 μg/mL ampicillin, and 100 μg/mL streptomycin. All cell cultures were done at 37°C under 5% CO_2.

Perineural invasion models in mice. NOD/SCID (NOD/LtSz-scid) mice were maintained in a specific pathogen-free environment. Eight- to 12-week-old mice were used in this experiment. The studies were conducted in accordance with the NIH Guide for the Care and Use of Laboratory Animals.

The human nerve perineural invasion models were prepared as follows. The human nerve plexus around the celiac axis or superior mesenteric artery were obtained from autopsies done until about 6 hours after death in sterile conditions, immediately placed in RPMI 1640 with antibiotics, divided into 1-cm pieces (about 0.25 cm^3), and kept in the medium for a brief period until transplantation. The divided tissue was placed in the s.c. space of NOD/SCID mice under anesthesia. After 4 weeks, each mouse received an injection of a pancreatic cancer cell line near the s.c. transplanted tissue with 7×10^6 viable tumor cells, which were harvested from subconfluent cultures, under the appropriate anesthetic procedure. Five to 8 weeks later, when the tumor grew up to about 1.5 cm in long diameter, after inoculation, mice were sacrificed, and autopsies were done immediately. The s.c. tissue was removed, fixed in 10% formalin, cut into 2- to 3-mm-thick slices, and embedded in paraffin. The samples were processed for histologic examination.

The mouse nerve perineural invasion models were prepared as follows. Each mouse received a s.c. injection of 7×10^6 viable pancreatic cancer cells on the midline of the mouse's back and processed by the same protocol as above. All animals tolerated each procedure well.

RNA preparation and oligonucleotide array. Total RNA was extracted from cells with an RNAeasy Mini kit (Qiagen, Hilden, Germany). According to the manufacturer's protocol (Affymetrix, Santa Clara, CA), biotin-labeled cRNA was synthesized from 5 mg of total RNA, hybridized to the GeneChip HG-U133A, stained with streptavidin-phycoerythrin, and then detected by scanning. Each of the scanned images was normalized as mean signal intensity of all probe sets at 1,000. Two-dimensional clustering analysis using the standard correlation as a similarity measure was done by the software, GeneSpring version 6.2 (Silicon Genetics, Redwood City, CA).

Real-time quantitative reverse transcription-PCR analysis. Real-time quantitative reverse transcription-PCR (RT-PCR) analysis was done as follows. The primer set 5′-GACCTTATCTCCAACAATGAGCAAC-3′ (forward) and 5′-AGCAGAGTCACCAGGATGGAA-3′ (reverse) was used for CD74. To standardize the amount of RNA, expression of

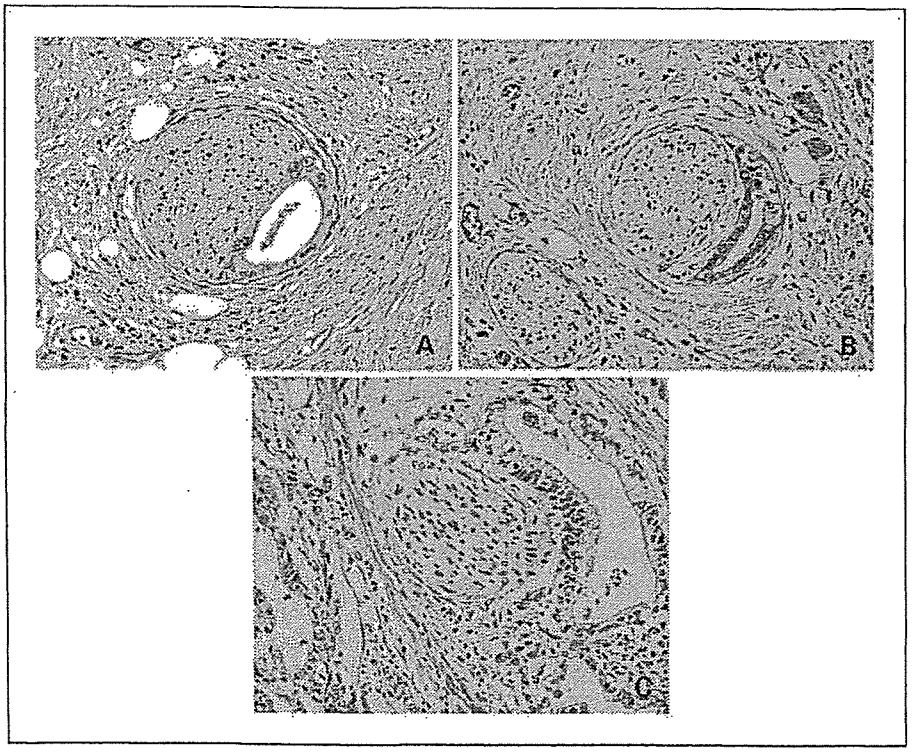

Fig. 1. Three patterns of relationships between cancer cells and peripheral nerves. Perineural invasion: cancer cells invaded to the perineural space between the perineurium and endoneurium of the peripheral nerve with direct contact with the endoneurium (*A*). Epineural invasion: cancer cell invaded along the perineurium without contact with the endoneurium (*B*). Nerve involvement: cancer nests included nerves without direct mutual contact (*C*). H&E; magnification × 200.

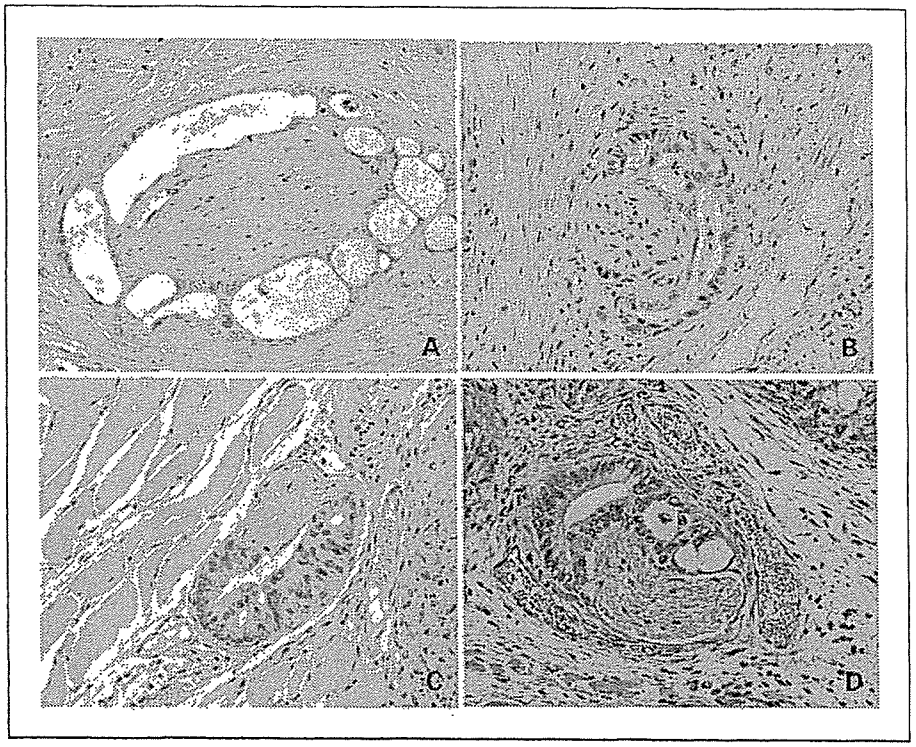

Fig. 2. Perineural invasion to human and mouse nerves. Perineural invasion in a human nerve perineural invasion model (*A*, CaPan2; *B*, CFPAC) and perineural invasion in a mouse nerve perineural invasion model (*C*, CaPan1; *D*, CaPan2). H&E; magnification × 200.

glyceraldehyde-3-phosphate dehydrogenase in each sample was quantified by using the primer set 5′-GCACCGTCAAGGCTGAGAAC-3′ (forward) and 5′-ATGGTGGTGAAGACGCCAGT-3′ (reverse), and the amount of CD74 expression was divided by that of the glyceraldehyde-3-phosphate dehydrogenase in each sample. All PCR reactions were done under the following conditions: one cycle at 95°C for 10 seconds and then 40 cycles at 95°C for 5 seconds and 60°C for 30 seconds. Real-time detection of the emission intensity of SYBR Green (Qiagen) was done using an ABI prism 7000 Sequence Detector (Perkin-Elmer Applied Biosystems, Foster city, CA), using a previously reported method (19). Quantitative RT-PCR was done at least thrice.

Western blotting. All 20-μg cell lysates were subjected to 10% SDS-PAGE and then separated proteins were transferred to Hybond-P (Amersham Biosciences, Buckinghamshire, United Kingdom). After blocking, an anti-CD74 mouse monoclonal antibody (LN 2; DAKO, Glostrup, Denmark) was used at a dilution of 1:1,000 overnight at 4°C. The membrane was incubated with a horseradish peroxidase–conjugated secondary antibody (DAKO) and visualized by using an enhanced chemiluminescence kit (Amersham Biosciences). A Burkitt's lymphoma (Raji) cell line was used as a positive control for CD74.

Immunofluorescence. CaPan2 cell lines were grown on glasses and fixed in 8% paraformaldehyde for 20 minutes on ice. They were incubated with an anti-CD74 antibody for 1 hour followed by a FITC-labeled secondary antibody (DAKO). Texas Red-X phalloidin (Molecule Probes, Eugene, OR) was used to visualize filamentous-actin. Slides were examined using an Olympus fluorescence microscope with a MRC-600 scanning laser confocal apparatus (Olympus, Tokyo, Japan).

Patients and tissue samples. For immunohistochemical analysis, 67 invasive ductal pancreas adenocarcinomas were analyzed. Sections were prepared from formalin-fixed, paraffin-embedded tissues of samples resected surgically between 1991 and 2004. This study was conducted under the approval of the Ethics Committee of Keio University, School of Medicine. Histologic diagnoses were made according to WHO criteria or the Japan pancreas society classification (20). Perineural invasion, which was frequently observed in surgical specimens, was defined as cancer cell invasion to the perineural space between the perineurium and endoneurium of the peripheral nerve with direct contact to the endoneurium (Fig. 1A), whereas epineural invasion, where cancer cells invade along the perineurium without contact to the endoneurium (Fig. 1B), and nerve involvement, where a cancer nest included nerves without direct contact between them (Fig. 1C), were excluded from perineural invasion (21). Intraneural invasion was also included in perineural invasion.

The degree of perineural invasion was defined microscopically as follows: 0, no perineural invasion; 1, perineural invasion was difficult to find with only one to three occurrences in the lesions; 2,

Table 1. Incidence of perineural invasion in mouse nerve perineural invasion models

	CaPan1	CaPan2	HPAFII	AsPC1	Panc1	*P**
No. mice examined	11	13	11	11	5	
Perineural invasion	6†	9	0	0	0	0.000004
Epineural invasion	3	6	3	4	0	0.216
Nerve involvement	6	8	5	7	3	0.615

*CaPan1 and CaPan2 vs HPAFII, AsPC1, and Panc1.
†Each value indicates the number of mice where perineural invasion, epineural invasion, and nerve involvement was observed, respectively.

perineural invasion was easy to find, in between 1 and 3; and 3, perineural invasion was even easier to find, with more massive occurrences in the lesions and extension beyond the border of the main tumor mass.

Immunohistochemistry. Each section was deparaffinized, rehydrated, and incubated with fresh 0.3% hydrogen peroxide in methanol for 30 minutes at room temperature and then heated in 10 mmol/L citrate buffer (pH 6) for 10 minutes after washing in PBS. Normal goat serum (Invitrogen, Carlsbad, CA) was applied for 30 minutes and removed. The section was then incubated with anti-CD74 antibody at a dilution of 1:100 overnight at 4°C, washed thrice in PBS, and incubated with a secondary antibody for 30 minutes at room temperature. A simple stain MAX-PO (Nichirei, Tokyo, Japan) was used to detect the antibody signals as the secondary antibody. Staining was evaluated by three independent observers (N.K., R.S., and M.S.). An equal staining to lymphocytes was considered positive. The positivity index was expressed as the percentage of positive cancer cells in each lesion. The cases with ≥10% positive cells were defined as CD74 positive.

Statistical analysis. Data are expressed as mean ± SD. The level of CD74 mRNA in the high and low perineural invasion groups was compared using the Mann-Whitney *U* test. The other correlations were analyzed by the χ^2 test. All statistical analyses were done using Statcel2 (OMS Publisher, Saitama, Japan). The results were judged significant at $P < 0.05$.

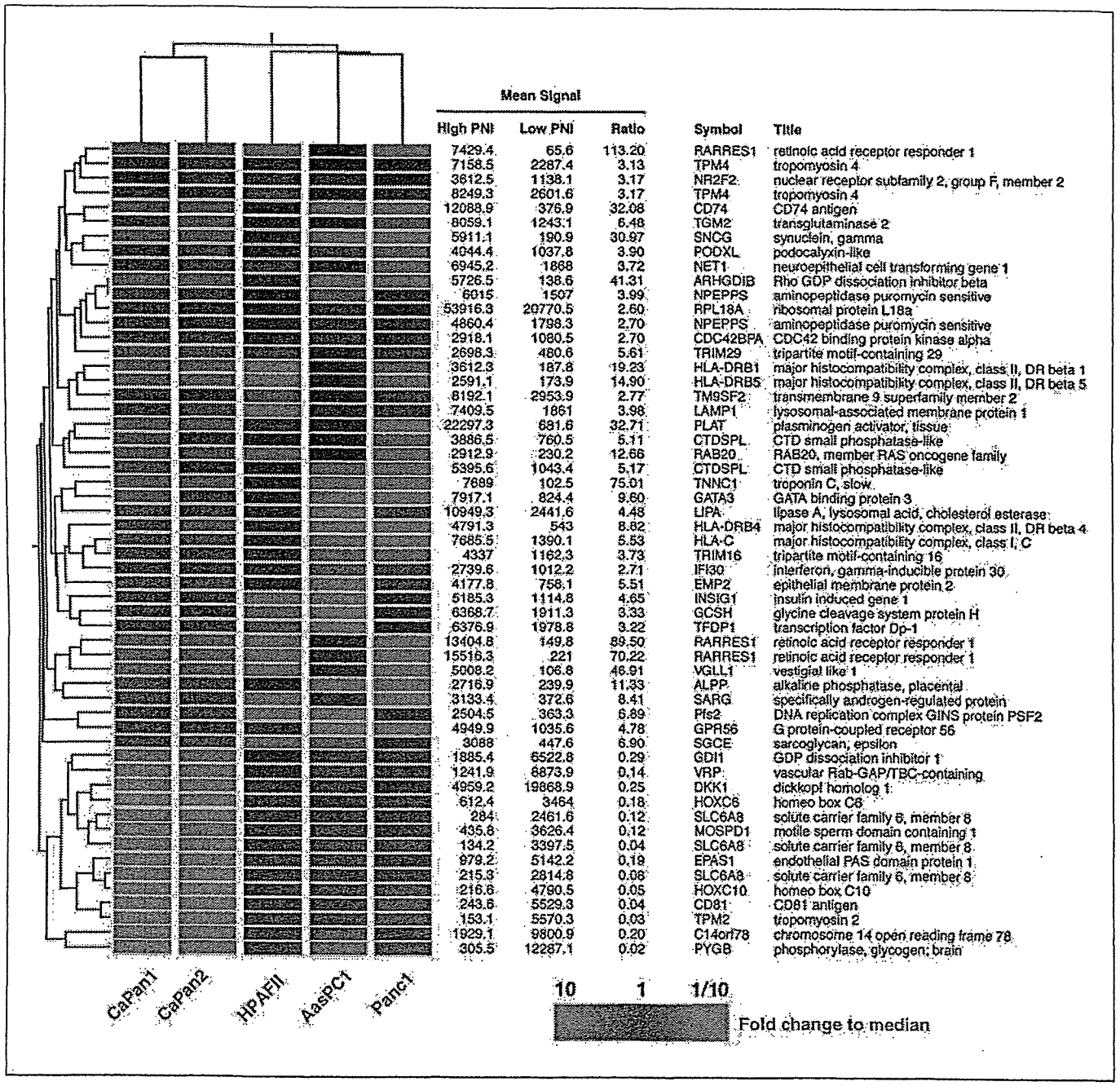

Fig. 3. Two-way hierarchical clustering algolithm. Forty-nine genes displayed a ≥2-fold increase or decrease in expression level. Each color patch in the resulting visual map represents the expression level of the associated gene in the cell line sample, with a continuum of expression levels from *green* (lowest) to *bright red* (highest). A two-way hierarchical clustering algorithm successfully distinguished between the high and low perineural invasion groups. The scale bar reflects the fold increase (*red*) or decrease (*green*) for any given gene relative to the median level of expression across all samples.

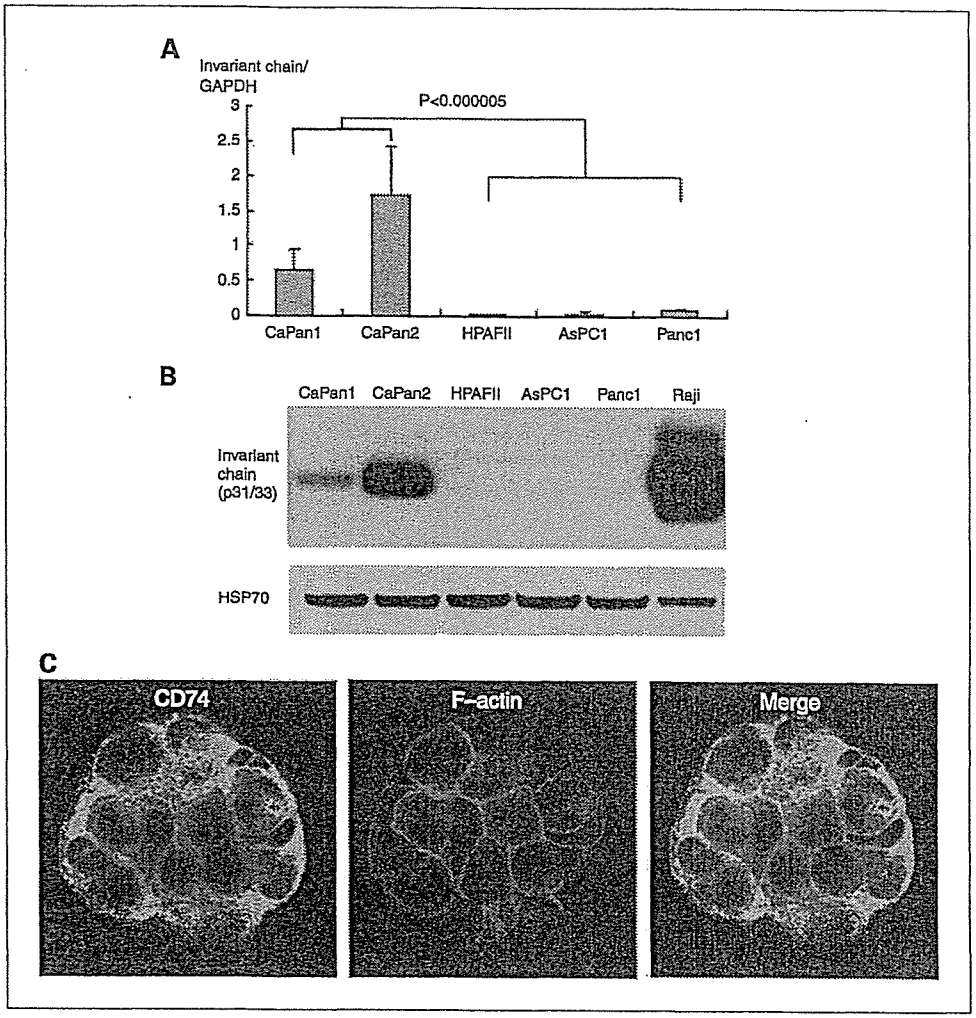

Fig. 4. CD74 expression in pancreatic cancer cell lines. *A*, real-time quantitative RT-PCR analysis of CD74. The expression levels were normalized with glyceraldehyde-3-phosphate dehydrogenase (*GAPDH*) mRNA in each sample. *B*, Western blotting analysis of the CD74 protein. Each cell lysate (20 μg) was analyzed using an anti-CD74 antibody. HSP70 was used as an internal control. *C*, immunofluorescence analysis of CD74 and filamentous actin (*F-actin*) in CaPan2. CaPan2 cells were stained for CD74 (*green*) and filamentous actin (*red*).

Results

Subcutaneous implantation of pancreatic cancer cell lines. To analyze the potential of perineural invasion, seven pancreatic cancer cell lines were s.c. implanted in NOD/SCID mice with human nerve tissue. CaPan1, CaPan2, CFPAC, and MPanc96 showed perineural invasion to human nerves (Fig. 2A and B). Therefore, we confirmed that even cell lines preserved their ability to show perineural invasion to human nerve–like clinical cases. However, pancreatic cancer cell lines frequently did not invade to the transplanted human nerve tissue, probably due to the adverse effect of accompanying inflammatory cells in nerve tissue. Thus, it was difficult to evaluate these models quantitatively. Because we observed these cells also presented perineural invasion to mouse s.c. peripheral nerves (Fig. 2C and D), we employed mouse nerve perineural invasion models for further analyses of perineural invasion.

To analyze quantitatively the frequency of perineural invasion of pancreatic cancer cell lines in mouse s.c. nerves, we selected five cell lines (CaPan1, CaPan2, HPAFII, AsPC1, and Panc1) and implanted these cell lines in the s.c. tissue of 5 to 13 NOD/SCID mice and analyzed the frequency of neural invasion to the mouse s.c. nerves. Perineural invasion of CaPan1 and CaPan2 cells was seen in 6 of 11 and 9 of 13 implanted mice, respectively. In contrast, the other three cell lines did not show perineural invasion, whereas each cell line showed epineural invasion and nerve involvement to the mouse s.c. nerves. These findings indicated that CaPan1 and CaPan2 (high perineural invasion group) had greater potential for perineural invasion *in vivo*, whereas the other three cell lines (low perineural invasion group) had little potential for perineural invasion ($P < 0.000004$; Table 1).

Two-way hierarchical clustering algorithm. To identify genes generally involved in perineural invasion, we compared the expression profiles of the high and low perineural invasion groups. We filtered all genes, with the following limits: (*a*) presence with signal at >2,000; (*b*) >2-fold increase or decrease in average difference between each high perineural invasion cell line and the low perineural invasion group and the high perineural invasion group and each low perineural invasion cell line. In the 49 genes selected under the above criteria, 37 were up-regulated, and 12 were down-regulated in the high perineural invasion group compared with the low perineural invasion group. A two-way hierarchical clustering algorithm successfully distinguished between the high and low perineural invasion groups (Fig. 3).

CD74 expression in pancreatic cancer cell lines. From the genes listed in Fig. 3, we further investigated *CD74*, because it was one of the most highly expressed genes in the high perineural invasion group and is thought to be a membrane